

37 1. Introduction

38

39 The cycling of nitrogen (N) in the upper ocean is central to the role that phytoplankton and bacteria play
40 in atmospheric carbon dioxide (CO₂) consumption and production. Annually, the Southern Ocean
41 accounts for ~35% of total oceanic CO₂ removal (DeVries et al., 2017; Gruber et al., 2019; Watson et
42 al., 2020) and absorbs ~40% of anthropogenic CO₂ (Khaliwala et al., 2009; Hauck et al., 2015; Gruber
43 et al., 2019; Watson et al., 2020). The contribution of biology to CO₂ drawdown can be evaluated using
44 the new production paradigm, among other approaches. This framework defines phytoplankton growth
45 on nitrate (NO₃⁻) supplied from below the euphotic zone as “new production” and phytoplankton growth
46 on ammonium (NH₄⁺) recycled within the euphotic zone as “regenerated production” (Dugdale and
47 Goering 1967). Over appropriate timescales, new production is equivalent to “export production”, the
48 latter referring to the organic matter produced by phytoplankton that escapes recycling in surface waters
49 and sinks into the ocean interior, thereby sequestering atmospheric CO₂ at depth (Dugdale and Goering,
50 1967; Eppley and Peterson, 1979; Volk and Hoffert, 1985; Raven and Falkowski, 1999). The occurrence
51 of nitrification in the euphotic zone, which produces regenerated NO₃⁻, complicates applications of the
52 new production paradigm since phytoplankton growth fuelled by this NO₃⁻ will drive no net removal of
53 CO₂ (Yool et al., 2007).

54

55 In the Southern Ocean, nitrification appears to be largely confined to the dark waters below the euphotic
56 zone during the summertime period of maximum NO₃⁻ consumption by phytoplankton (DiFiore et al.,
57 2009; Mduyana et al., 2020). By contrast, the Southern Ocean winter is characterized by elevated
58 mixed-layer nitrification rates, coincident with low rates of NO₃⁻ uptake (Smart et al., 2015; Mduyana
59 et al., 2020). Some of the NO₃⁻ regenerated in the winter mixed layer will be supplied to phytoplankton
60 during the proceeding spring and summer growing season, with negative implications for CO₂ removal
61 on an annual basis. That said, there is evidence that ammonia oxidizing archaea, the organisms that are
62 dominantly responsible for NH₄⁺ oxidation (the first step in the nitrification pathway) (Beman et al.,
63 2008; Newell et al., 2011; Peng et al., 2016) have a high iron requirement (Shafiee et al., 2019), such
64 that NH₄⁺ oxidation may at times experience iron limitation (Mduyana et al. 2022). If this limitation
65 is verified and proves widespread in the environment, one implication is that the iron-deplete conditions
66 of the surface Southern Ocean may restrict mixed-layer nitrification and by extension, decrease the
67 extent to which phytoplankton growth is fueled by regenerated nitrate.

68

69 Nitrification is a chemoautotrophic process involving two pathways usually facilitated by different
70 groups of microorganisms. The first step is NH₄⁺ oxidation, which involves the oxidation of NH₄⁺ via
71 hydroxylamine and nitric oxide to NO₂⁻ (Walker et al. 2010; Vajjala et al. 2013; Kozłowski et al. 2016;
72 Caranto and Lancaster 2017) by ammonia oxidizing archaea and bacteria (AOA and AOB, respectively;
73 collectively, ammonia oxidizing organisms, AOO). The second step is the oxidation of NO₂⁻ to NO₃⁻ by

74 nitrite oxidizing bacteria (NOB), a polyphyletic group of microbes that is not well-understood in the
75 ocean (Watson et al., 1986; Beman et al., 2013; Daims et al., 2016; Pachiadaki et al., 2017; Sun et al.,
76 2021). In general, NO_2^- oxidation rate data are limited, with few measurements available for the
77 Southern Ocean (Bianchi et al. 1997; Mdotyana et al. 2020; Olson 1981a). Such measurements are
78 critical, however, if we are to better understand the controls on nitrification in the Southern Ocean
79 mixed layer and the connection between NO_3^- production by NOB and its subsequent removal by
80 phytoplankton.

81

82 One approach for investigating the controls on NO_2^- oxidation is through experiments designed to yield
83 a hyperbolic Michaelis-Menten relationship between NO_2^- oxidation rate and NO_2^- concentration.
84 Useful kinetic parameters can be derived from this relationship, such as the maximum oxidation rate
85 (V_{max}) and the half-saturation constant (K_m), with the latter indicating the NO_2^- concentration at which
86 the oxidation rate equals $V_{\text{max}}/2$. Estimates of K_m provide information regarding the efficiency of NOB
87 in acquiring substrate NO_2^- , with a lower K_m indicating a higher affinity for NO_2^- , while V_{max} denotes
88 the maximum rate of NO_2^- oxidation that can be achieved under a given set of conditions by a particular
89 NOB community. In the ocean, direct measurements of NO_2^- oxidation kinetic parameters are extremely
90 limited (Olson, 1981; Sun et al., 2017, 2021; Zhang et al., 2020), with no estimates available for the
91 Southern Ocean. K_m values derived from culture studies of NOB range from 9-544 μM (Nowka et al.,
92 2015; Ushiki et al., 2017), orders of magnitude higher than the existing estimates for natural
93 assemblages of NOB in coastal waters and oxygen deficient zones (ranging from 0.07-0.51 μM ; Olson,
94 1981; Sun et al., 2017; Zhang et al., 2020). This discrepancy emphasizes the gaps in our understanding
95 of NO_2^- oxidation and the organisms that catalyse it.

96

97 Generally, NO_2^- concentrations in the low-latitude oxygenated ocean reach a maximum near the base
98 of the euphotic zone (i.e., the primary nitrite maximum; PNM), with much lower concentrations above
99 and below this depth (Lomas and Lipschultz 2006). By contrast, at higher latitudes including in the
100 Southern Ocean, the NO_2^- concentrations are elevated (100-400 nM) and fairly invariant throughout the
101 mixed layer in all seasons (Zakem et al. 2018; Fripiat et al. 2019; Mdotyana et al. 2020). A possible
102 explanation for this NO_2^- accumulation is a decoupling of the NH_4^+ and NO_2^- oxidation rates, with NO_2^-
103 oxidation being the rate-limiting step in the nitrification pathway, contrary to expectations for
104 oxygenated marine waters (Kendall, 1998; Walker et al., 2010; Vajrala et al., 2013). However, this idea
105 has yet to be examined using observations.

106

107 To better understand the controls on NO_2^- oxidation (and thus, nitrification) in the Southern Ocean, we
108 conducted a series of NO_2^- oxidation kinetics experiments in wintertime surface waters across the
109 western Indian sector. At every station (seven in total) along a transect between the Subtropical and
110 Marginal Ice Zones, NO_2^- oxidation rates increased with increasing NO_2^- concentrations, as per the

111 expected Michaelis-Menten relationship. The derived K_m values were low and increased with increasing
112 ambient NO_2^- . Additionally, there appeared to be a minimum NO_2^- concentration that was required
113 before the NO_2^- oxidation rates increased significantly, implying a “threshold” NO_2^- requirement for
114 NO_2^- oxidation in the Southern Ocean. Finally, coincident measurements of euphotic zone NH_4^+ and
115 NO_2^- oxidation rates suggest that NO_2^- oxidation is rate-limiting for nitrification across the Southern
116 Ocean in winter.

117

118 **2. Materials and Methods**

119

120 **2.1. Sampling site and experimental design**

121 A winter cruise was undertaken onboard the R/V *SA Agulhas II* in July 2017 between Cape Town, South
122 Africa, and the Marginal Ice Zone (MIZ; encountered at 61.7°S; de Jong et al., 2018), returning to South
123 Africa along the meridional WOCE I06 transect (30°E) (Figure 1). Sampling was conducted on two
124 legs – between 37°S and 62°S on the southward leg (Leg 1) and between 59°S and 41°S on the
125 northward return leg along the WOCE I06 line (Leg 2). During Leg 1, only surface samples were
126 collected while on Leg 2, the deployment of conductivity-temperature-depth (CTD) hydrocasts allowed
127 for depth-profile sampling.

128

129 *2.1.1 Hydrography and nutrient collections:* The positions of the major hydrographic fronts (the
130 Subtropical Front, STF; Subantarctic Front, SAF; Polar Front, PF; and Southern Antarctic Circumpolar
131 Current Front, SACCF; Figure 1) were determined from temperature and salinity measured by the ship’s
132 hull-mounted thermosalinograph (~7 m), augmented by temperature, salinity, and oxygen
133 concentrations measured on Leg 2 by the CTD sensors (Orsi et al., 1995; Belkin and Gordon, 1996;
134 Pollard et al., 2002; Read et al., 2002). For the hydrocast stations, the mixed layer depth was determined
135 for each CTD (up)cast as the depth between 10 m and 400 m of maximum Brunt Väisälä frequency
136 squared (i.e., N^2) (Schofield et al., 2015; Carvalho et al., 2017). Surface photosynthetically active
137 radiation (PAR) was not measured continuously during the cruise; we thus use latitude as a qualitative
138 proxy for light availability during Leg 1.

139

140

141 *2.1.2 Nutrient samples:* Seawater samples were collected every four hours from the ship’s underway
142 system (~7 m intake) on Leg 1 for the determination of NO_2^- concentrations (Figure 1a). During Leg 2,
143 samples were collected from Niskin bottles fired remotely between the surface and 500 m at eight
144 hydrocast stations for the analysis of NO_2^- , NO_3^- , and NH_4^+ concentrations (see Figure 1b and c for
145 station locations and sampling depths). For NO_2^- and NO_3^- , unfiltered seawater was collected in
146 duplicate 50 mL polypropylene centrifuge tubes that were analysed shipboard within 24 hours of
147 collection (NO_2^-) or stored frozen at -20°C until analysis (NO_3^-). Seawater samples for NH_4^+ were

148 collected unfiltered in duplicate high-density polyethylene (HDPE) bottles that had been “aged” with
149 orthophthaldialdehyde (OPA) working reagent, and analysed shipboard within 24 hours of collection.

150

151 *2.1.3 NO₂⁻ oxidation kinetics experiments:* On Leg 1, seawater samples were collected from the surface
152 via the ship’s underway system at seven stations spanning the different zones of the Southern Ocean
153 (the Subtropical Zone (STZ) to the north of the STF, at the STF, the Subantarctic Zone (SAZ) between
154 the STF and SAF, the Polar Frontal Zone (PFZ) between the SAF and PF, the Open Antarctic Zone
155 (OAZ) between the PF and SACCF, and the Marginal Ice Zone (MIZ) south of the SACCF; St 01 to St
156 07 in Figure 1a). At each station, 25 L of seawater were collected in a single carboy that was gently
157 shaken to homogenize the contents before the seawater was filtered through a 200 µm nylon mesh to
158 remove zooplankton grazers and then dispensed into 250 mL acid-washed opaque HDPE bottles. All
159 the bottles were rinsed three times with sample water prior to filling. Eight sets of duplicate 250 mL
160 bottles were amended with Na¹⁵NO₂ to yield ¹⁵NO₂⁻ concentrations ranging from 10 nM to 1500 nM.

161

162 *2.1.4 Depth distribution of NO₂⁻ oxidation:* On Leg 2, seawater was collected at four stations (one each
163 in the Polar Antarctic Zone (PAZ; just north of the edge of the MIZ), OAZ, PFZ, and SAZ; St 08 to St
164 11 in Figure 1a-c) using a CTD-rosette equipped with 24 12-L Niskin bottles. Seawater from six depths
165 (10 m, 25 m, 50 m, 75 m, 200 m, and 500 m) was pre-filtered (200 µm nylon mesh) and transferred into
166 rinsed 250 mL acid-washed opaque HDPE bottles. Duplicate bottles from each depth were amended
167 with Na¹⁵NO₂ to yield a final ¹⁵NO₂⁻ concentration of 200 nM. From all incubation bottles (for kinetics
168 and depth-profile experiments), initial (T₀) subsamples were collected in 50 mL centrifuge tubes
169 immediately after the addition of ¹⁵NO₂⁻. The opaque HDPE bottles from the upper 75 m were then
170 incubated in custom-built on-deck incubators supplied with running surface seawater, while those from
171 200 m and 500 m were incubated in a ~2°C cold room. The incubations lasted 23-30 hours and were
172 terminated via the collection of final (T_f) subsamples (50 mL). Subsamples were filtered (0.2 µm) and
173 stored frozen at -20°C until analysis.

174

175 *2.1.5 Depth distribution of NO₃⁻ uptake:* To assess the extent to which mixed-layer NO₂⁻ oxidation
176 supports wintertime NO₃⁻ uptake by phytoplankton, we also conducted NO₃⁻ uptake experiments over
177 the upper 75 m (the approximate depth of the euphotic zone) at St 08 to St 11 on Leg 2. Seawater was
178 collected from four depths – 10 m, 25 m, 50 m, and 75 m – in duplicate 2 L clear polycarbonate bottles
179 following filtration (200 µm nylon mesh) to remove large zooplankton grazers. Na¹⁵NO₃ was added to
180 each bottle to yield a final ¹⁵NO₃⁻ concentration of 3 µM, and the bottles were then transferred to custom-
181 built deck-board incubators equipped with neutral density screens that allowed for the penetration of
182 55%, 30%, 10%, and 1% of surface PAR. The bottles were kept at near *in situ* temperature via a supply
183 of continuously-running seawater from the underway system. Samples were incubated for 3-6 hours,
184 and incubations were terminated by filtering the bottle contents through pre-combusted (450°C for 8

185 hours) 0.3 μm glass fibre filters (GF-75; Sterlitech) that were subsequently enclosed in foil envelopes
186 (pre-combusted at 500°C for 5 hours) and stored at -80°C until analysis.

187

188 2.2. Laboratory analyses

189 *2.2.1 Nutrient concentrations:* Samples were analysed shipboard for NO_2^- concentrations using the
190 colorimetric method of Grasshoff et al., (1983) and a Thermo Scientific Genesys 30 Visible
191 spectrophotometer (detection limit of 20 nM, precision of ± 20 nM). $\text{NO}_3^- + \text{NO}_2^-$ concentrations were
192 measured ashore using a Lachat Quick-Chem flow injection autoanalyzer (Egan, 2008) in a
193 configuration with a detection limit of 0.2 μM and precision of ± 0.3 μM . The concentration of NO_3^-
194 was determined by subtracting NO_2^- from $\text{NO}_3^- + \text{NO}_2^-$. Aliquots of a certified reference material
195 (JAMSTEC) were included in each NO_2^- and $\text{NO}_3^- + \text{NO}_2^-$ run to ensure measurement accuracy. The
196 NH_4^+ concentrations were also determined shipboard using the fluorometric method of Holmes et al.
197 (1999); the methodological details and NH_4^+ data are discussed at length in (Mdutyana 2021) and (Smith
198 et al., (2022)).

199

200 *2.2.2 NO_2^- oxidation rates:* Using the denitrifier-isotope ratio mass spectrometer (IRMS) method
201 (Sigman et al., 2001; Weigand et al., 2016), we measured the $\delta^{15}\text{N}$ of NO_3^- ($\delta^{15}\text{N}\text{-NO}_3^-$) produced from
202 $^{15}\text{NO}_2^-$ oxidation for both the kinetics and depth-profile experiments ($\delta^{15}\text{N}$, in ‰ vs. air, =
203 $(^{15}\text{N}/^{14}\text{N}_{\text{sample}}/^{15}\text{N}/^{14}\text{N}_{\text{air}} - 1) \times 1000$). Samples were measured using a Delta V Plus IRMS with a custom-
204 built purge-and-trap front end (Weigand et al., 2016) in a configuration with a detection limit of 0.2
205 nmol of N and a $\delta^{15}\text{N}$ precision of 0.2‰. Prior to isotope analysis, samples were treated with sulfamic
206 acid (15 mM) to remove $^{15}\text{NO}_2^-$ remaining at the end of the experiments, after which sample pH was
207 adjusted to ~7-8 via the addition of 2 M NaOH. To account for inefficiencies in $^{15}\text{NO}_2^-$ removal, both
208 the T_f and T_0 samples were treated with sulfamic acid prior to analysis of $\delta^{15}\text{N}\text{-NO}_3^-$ (more accurately,
209 $\delta^{15}\text{N}\text{-NO}_3^- + \text{NO}_2^-$), with the difference between them taken as the $^{15}\text{NO}_3^-$ enrichment due to $^{15}\text{NO}_2^-$
210 oxidation (Peng et al., 2015). International reference materials (IAEA-N3, USGS 34, USGS 32) were
211 used to calibrate the measured $\delta^{15}\text{N}\text{-NO}_3^-$.

212

213 The rate of NO_2^- oxidation ($\text{NO}_2^-_{\text{ox}}$; nM d⁻¹) was calculated following Peng et al., (2015) as:

214

$$215 \quad \text{NO}_2^-_{\text{ox}} = \frac{\Delta[^{15}\text{NO}_3^-]}{f_{\text{NO}_2^-}^{15} \times T} \quad (1)$$

216

217 Where $\Delta[^{15}\text{NO}_3^-]$ is the change in the concentration of $^{15}\text{NO}_3^-$ between the start and end of the incubation
218 due to NO_2^- oxidation, calculated from the difference in the measured $\delta^{15}\text{N}\text{-NO}_3^-$ between the T_f and T_0
219 samples, $f_{\text{NO}_2^-}^{15}$ is the fraction of the NO_2^- substrate pool labelled with ^{15}N at the start of the incubation,

220 calculated following the direct measurement of ambient NO_2^- concentration, and T is the incubation
221 length (days). Detection limits for NO_2^- ox rates ranged from 0.11 to 0.36 nM d^{-1} , calculated according
222 to Santoro et al. (2013) and Mdutyana et al. (2020).

223

224 *2.2.3 Kinetic model:* Kinetic parameters are typically calculated using the Michaelis-Menten (MM)
225 equation for enzyme kinetics (Monod, 1942):

226

$$227 \quad V = \frac{V_{\max} \times S}{K_m + S} \quad (2)$$

228

229 where V is the measured reaction rate, V_{\max} is the maximum reaction rate achievable under *in situ*
230 conditions at saturating substrate (S) concentrations, and K_m is the half-saturation constant, defined as
231 the substrate concentration at which $V = V_{\max}/2$.

232

233 The MM equation (equation 2) is a rectangular hyperbola, meaning that the asymptotes along the x-
234 and y-axes are perpendicular. By definition, when S (the x-axis variable) is equal to zero, V (the y-axis
235 variable) is also zero, forcing the model through the origin (0,0). In the case of NO_2^- oxidation, the
236 assumption that once $S > 0$, $V > 0$ is appropriate in waters where the ambient NO_2^- concentration is
237 near-zero or where NO_2^- is non-zero but considerably lower than the K_m . In the Southern Ocean, mixed-
238 layer NO_2^- concentrations are typically ≥ 150 nM (Cavagna et al., 2015; Zakem et al., 2018; Fripiat et
239 al., 2019; Mdutyana et al., 2020) and forcing the MM model through the origin results in a poor fit to
240 the measurements (red line in Figure S1). This poor fit, in turn, leads to clearly inaccurate estimates of
241 the kinetic parameters, particularly K_m (Table S1).

242

243 While not typical for studies of NO_2^- oxidation kinetics in the ocean, the standard form of non-linear
244 regression models, including the MM equation, can be modified to better fit the observations (e.g.,
245 Birch, 1999; Tsoularis and Wallace, 2002; Archontoulis and Miguez, 2014). For application to our
246 dataset, we modified equation 2 to allow $V = 0$ at $S > 0$ by subtracting a location parameter, C, from S
247 (Figure 2) (Archontoulis and Miguez, 2014). In other words, we set the y-intercept (i.e., where $V = 0$)
248 equal to C rather than to zero, which yields equation 3:

249

$$250 \quad V = \frac{V_{\max} \times (S-C)}{K_{m^*} + (S-C)} \quad (3)$$

251

252 Using a non-linear, least-squares optimization method (Scipy lmfit package, Python 3.7.6), we solved
253 equation 3 for V_{\max} , K_{m^*} , and C. The value of K_{m^*} derived in this way is relative to C, such that the
254 substrate concentration at which $V = V_{\max}/2$ (i.e., K_m) is actually equal to $K_{m^*} + C$ (Supplemental
255 Information). Mechanistically, C represents a “threshold” substrate concentration; when $S \leq C$, $V = 0$.

256 All derived kinetic parameters are reported as the best fit plus 95% confidence interval (i.e., mean \pm 2 σ ;
257 Table 1).

258

259 *2.2.4 Revising the depth distribution of NO₂⁻ oxidation using K_m:* For the NO₂⁻ oxidation experiments
260 conducted at the Leg 2 hydrocast stations (i.e., depth-profile experiments; St 08 to St 11), the Na¹⁵NO₂
261 was added to yield a final ¹⁵NO₂⁻ concentration of 200 nM at all the sampled depths. However, at low
262 ambient NO₂⁻ concentrations (<1-2 μ M), an amendment of this magnitude may stimulate NO₂⁻
263 oxidation, leading to an overestimation of the *in-situ* rates. We thus revised our measured NO₂⁻ ox rates
264 using the derived K_m values as per Rees et al. (1999), Diaz and Raimbault, (2000), and Horak et al.
265 (2013):

266

$$267 \text{ corrNO}_2^-_{\text{ox}} = \frac{\text{NO}_2^-_{\text{ox}}}{\frac{[\text{NO}_2^-]_{\text{total}}}{K_m + [\text{NO}_2^-]_{\text{total}}} \times \frac{K_m + [\text{NO}_2^-]_{\text{amb}}}{[\text{NO}_2^-]_{\text{amb}}}} \quad (4)$$

268

269 Here, corrNO₂⁻ ox is the revised rate of NO₂⁻ ox, NO₂⁻ ox is the measured NO₂⁻ oxidation rate (equation 1),
270 [NO₂⁻]_{amb} is the ambient NO₂⁻ concentration measured at each depth, [NO₂⁻]_{total} refers to the
271 concentration of ¹⁵NO₂⁻ tracer plus NO₂⁻ amb, and K_m is the derived half-saturation constant. We estimated
272 a K_m for each sample depth from the equation resulting from the linear regression of all derived K_m
273 values on [NO₂⁻]_{amb} (see section 4.2 below). We also computed corrNO₂⁻ ox using the K_m derived from
274 the Leg 1 kinetics experiment located nearest each hydrocast station, which yielded very similar results.
275 The values of corrNO₂⁻ ox presented here were computed using the K_m values derived from the linear
276 regression equation. Rates of NH₄⁺ oxidation measured coincident with NO₂⁻ ox on Leg 2 (see Mduyana
277 et al., 2022 were similarly revised (to yield corrNH₄⁺ ox) using the K_m values derived from kinetics
278 experiments conducted during Leg 1 of the cruise – for St 08 and 09, K_m =137 nM, for St 09, K_m = 67
279 nM, and for St 11, K_m = 28 nM.

280

281 *2.2.5 Isotopic dilution of ¹⁵NO₂⁻ by co-occurring NH₄⁺ oxidation:* The focus of this study is the second
282 step in the nitrification pathway. However, not only will NO₂⁻ have been consumed in our incubation
283 bottles (i.e., oxidized to NO₃⁻), but it will also have been produced by NH₄⁺ oxidation, the first step in
284 the nitrification pathway. For all of our NO₂⁻ oxidation rate experiments (kinetics and depth-profile),
285 we measured the coincident rates of NH₄⁺ oxidation (Mduyana et al., 2022), and these data can be used
286 to account for any dilution of the ¹⁵NO₂⁻ pool by ¹⁴NO₂⁻ produced from ¹⁴NH₄⁺ oxidation (following the
287 approach of Glibert et al. (1982, 1985) and Mulholland and Bernhardt (2005)). We found that isotopic
288 dilution in the mixed layer was minor because the ambient NO₂⁻ concentrations were reasonably high
289 (mean of 157 \pm 54 nM, range of 64 to 226 nM for all the depths at which experiments were conducted;
290 Figure 1a-b) and the NH₄⁺ oxidation rates were fairly low (mean of 13.4 \pm 4.0 nM d⁻¹, range of 7.8 to
291 22.0 nM d⁻¹; see Figure 3f-j for the depth profile rates and Mduyana et al., (2022) for the kinetics station

292 rates). Below the mixed layer where the ambient NO_2^- concentrations were near-zero, so too were the
293 NH_4^+ oxidation rates, which again resulted in minimal dilution of the $^{15}\text{NO}_2^-$ pool. Accounting for
294 isotope dilution increased the NO_2^- oxidation rates by 0 to 12% (mean of $3.9 \pm 0.3\%$ and median of 3.7
295 $\pm 0.3\%$), which is within the experimental error associated with the rate measurements; we thus consider
296 the effect of isotope dilution to be negligible

297

298 *2.2.6 Nitrate uptake rates:* On shore, the GF-75 filters were oven-dried at 45°C for 24 hours, then
299 pelletized into tin cups following the removal of unused peripheral filter. The concentration and isotopic
300 composition of the particulate organic N (PON) captured on the filters was analyzed using a Delta V
301 Plus IRMS coupled to a Flash 2000 elemental analyser, with a detection limit of $1 \mu\text{g N}$ and precision
302 of $\pm 0.005 \text{ At}\%$. Blanks (combusted unused filters + tin capsules) and laboratory running standards
303 calibrated to international reference materials were run after every five to ten samples. The absolute
304 rates of NO_3^- uptake (ρNO_3^- ; nM d^{-1}) were calculated after blank correction according to the equations
305 of Dugdale and Wilkerson (1986) assuming a day-length of between 7 and 10 hours, depending on the
306 station latitude. To compute the fraction of the mixed-layer NO_3^- pool consumed by phytoplankton that
307 derived from *in situ* nitrification, we trapezoidally-integrated ρNO_3^- and $\text{corrNO}_2^-_{\text{ox}}$ over the mixed layer
308 following Mduyana et al., (2020), and then divided the integrated values of $\text{corrNO}_2^-_{\text{ox}}$ by ρNO_3^- .

309

310 **3. Results**

311

312 **3.1 Hydrography and nutrient concentrations**

313 The positions of the major hydrographic fronts during both legs of the cruise are shown in Figure 1a.
314 At the hydrocast stations (Leg 2), the mixed layer depth (MLD) averaged 143 m in the OAZ, 146 m in
315 the PFZ, 205 m in the SAZ, and 113 m in the STZ, which is within the reported climatological range
316 for the western Indian sector of the Southern Ocean in winter (Sallée et al. 2010). Underway ambient
317 NO_2^- concentrations (Leg 1) ranged from 74 nM to 232 nM (transect average of $168 \pm 48 \text{ nM}$, median
318 of 177 nM) and generally increased with latitude, albeit with a high degree of variability (Figure 1a;
319 Figure S2). The ambient NO_2^- concentrations at the hydrocast stations were fairly constant throughout
320 the mixed layer (ranging from $55 \pm 35 \text{ nM}$ to $159 \pm 73 \text{ nM}$), decreasing rapidly to values below detection
321 by 150-200 m (Figure 1b). Mixed-layer NO_2^- showed no clear latitudinal trend, mainly because of the
322 anomalously low concentrations measured at St 09 (54°S ; mixed-layer average of $64 \pm 30 \text{ nM}$,
323 compared to 144 ± 56 for the seven other hydrocast stations). The NO_3^- concentrations were also near-
324 homogenous throughout the mixed layer, decreasing from an average of $28.4 \pm 0.2 \mu\text{M}$ at the
325 southernmost station (St 08; 59°S) to $3.7 \pm 1.1 \mu\text{M}$ at the northernmost station (41°S), and increasing
326 below the mixed layer as expected (Figure 1c).

327

328 **3.2. NO_2^- oxidation rates**

329 3.2.1 Kinetics experiments: At all the kinetics stations (St 01 to St 07; Leg 1), an MM curve could be
330 fit to the NO_2^- oxidation rate versus substrate concentration measurements using equation 3 (Figure 2).
331 The derived kinetic parameters varied across the transect (Table 1). The maximum NO_2^- oxidation rate
332 (V_{max}) increased southwards from $5.2 \pm 0.1 \text{ nM d}^{-1}$ at the STF (St 02; Figure 2b) to $13 \pm 0.4 \text{ nM d}^{-1}$ in
333 the AZ (St 05; Figure 2e), before decreasing in the MIZ to $8.2 \pm 0.1 \text{ nM d}^{-1}$ at St 06 (Figure 2f) and 6.6
334 $\pm 0.3 \text{ nM}$ at St 07 (Figure 2g). The average V_{max} for the transect was $9.0 \pm 1.1 \text{ nM d}^{-1}$. The half-saturation
335 constant (K_m) increased from $134 \pm 8.0 \text{ nM}$ at the STF (St 02) to $403 \pm 24 \text{ nM}$ in the MIZ (St 06), with
336 a transect average of $277 \pm 31 \text{ nM}$. The value of C showed a positive relationship with $[\text{NO}_2^-]_{\text{amb}}$ ($R^2 =$
337 0.59 ; $p = 0.045$) and no strong relationship with latitude, and ranged from $115 \pm 2.3 \text{ nM}$ at the STF (St
338 02) to $245 \pm 18 \text{ nM}$ in the A Z (St 05), with a transect average of $181 \pm 45 \text{ nM}$.

339

340 3.2.2 Depth-profile experiments: NO_2^- oxidation rates at St 08 to St 11, calculated using equation 1,
341 were low and largely invariant over the upper 75 m, ranging from 1.9 to 9.7 nM d^{-1} (average of $4.9 \pm$
342 2.4 nM d^{-1} ; filled symbols in Figure 3b-e). All stations showed a maximum NO_2^- oxidation rate at 200
343 m (roughly coincident with or just below the MLD), ranging between 11 and 28 nM d^{-1} (average of 18
344 $\pm 7.0 \text{ nM d}^{-1}$). The NO_2^- oxidation rates showed a latitudinal gradient, with lower rates in the AZ (St 08
345 and 09) than in the PFZ (St 10) and SAZ (St 11).

346

347 Revising the NO_2^- oxidation rates using equation 4 decreased their 0-75 m values by 13 to 26% (i.e.,
348 $\text{corrNO}_2^-_{\text{ox}}$ ranged from 1.6 to 8.5 nM d^{-1} and averaged $4.0 \pm 2.0 \text{ nM d}^{-1}$ over the upper 75 m; open
349 symbols in Figure 3b-e). The largest decrease (of 39 to 68%) occurred at 200 m and 500 m, coinciding
350 with the very low ambient NO_2^- concentrations (Figure 3a). Nonetheless, at all but St 08, the maximum
351 NO_2^- oxidation rate was still observed at 200 m, although its magnitude was lower. The coincidentally-
352 measured and revised NH_4^+ oxidation rates ($\text{corrNH}_4^+_{\text{ox}}$) showed a similar pattern, with the largest
353 decrease occurring at the depths with the lowest ambient NH_4^+ concentrations (Figure 3f-j) – over the
354 upper 75 m, the rates decreased by 1 to 9% at St 08 to St 10 where the mixed-layer NH_4^+ concentrations
355 averaged 263 ± 4.3 to $655 \pm 15 \text{ nM}$, while at St 11 where the mixed-layer NH_4^+ concentration averaged
356 $13 \pm 1.6 \text{ nM}$, the rates decreased by $40 \pm 23\%$. Similar to the NO_2^- oxidation rates, the NH_4^+ oxidation
357 rates decreased most at 200 m and 500 m, by between 33% and 70%. Hereafter, we use the revised NO_2^-
358 and NH_4^+ oxidation rates ($\text{corrNO}_2^-_{\text{ox}}$ and $\text{corrNH}_4^+_{\text{ox}}$, respectively) when referring to the depth
359 distributions of these processes, including in Figures 5 and 6. We note, however, that the revised rates
360 may still not be accurate since K_m was not derived individually for each depth at each station (Horak et
361 al., 2013). Nonetheless, because of the high concentration of the ^{15}N -tracer amendments relative to all
362 derived K_m values, we are confident that the revised rates are more representative of *in situ* conditions
363 than the rates computed using equation 1.

364

365 3.3 NO_3^- uptake rates

366 The rates of NO_3^- uptake (ρNO_3^-) were low and relatively homogenous over the upper 75 m at each
367 station (Figure S3a). Average euphotic zone ρNO_3^- increased northwards, from $2.9 \pm 1.1 \text{ nM d}^{-1}$ at St
368 08 in the AZ to $12 \pm 2.0 \text{ nM d}^{-1}$ at St 11 in the SAZ, with a transect average of $6.2 \pm 3.4 \text{ nM d}^{-1}$. The
369 euphotic zone PON concentrations also increased northwards, from $0.24 \pm 0.02 \text{ }\mu\text{M}$ at St 08 to $0.47 \pm$
370 $0.08 \text{ }\mu\text{M}$ at St 11 (Figure S3b). Integrated over the mixed layer, $\text{corrNO}_2^-_{\text{ox}}$ accounted for an average of
371 122% of ρNO_3^- (range of 63% at St 09 to 237% at St 08 in the AZ; Table S2), consistent with previous
372 observations from the wintertime Southern Ocean (Mdutyana et al., 2020).

373

374

375 4. Discussion

376 Across all the major zones of the wintertime Southern Ocean, the addition of NO_2^- to samples of surface
377 seawater stimulated NO_2^- oxidation following a Michaelis-Menten relationship, suggesting that
378 substrate availability plays a dominant role in determining the rate of NO_3^- production in the Southern
379 Ocean's winter mixed layer. Curiously, however, we also observed an apparent minimum substrate
380 requirement of NO_2^- oxidation (i.e., a "threshold" NO_2^- concentration, ranging from 115 to 245 nM),
381 which contradicts expectations for a "classical" Michaelis-Menten relationship (i.e., V is expected to
382 increase as soon as $S > 0$, assuming S is limiting to V ; Monod, 1942). Below, we examine our findings
383 in the context of existing estimates of NO_2^- oxidation kinetic parameters and then evaluate the potential
384 drivers of the trends that we observe. We also discuss possible reasons for the apparent requirement of
385 Southern Ocean NOB for a threshold ambient NO_2^- concentration and consider the implications thereof
386 for the regional N cycle.

387

388 4.1 Southern Ocean NO_2^- oxidation kinetic parameters in the context of existing estimates

389 Measurements of NO_2^- oxidation rates are limited in the Southern Ocean, with only two studies that
390 have directly measured this pathway in open-ocean waters (Bianchi et al. 1997; Mdutyana et al. 2020).
391 For NO_2^- oxidation kinetics, there are no data at all for the Southern Ocean. This scarcity of
392 measurements is unsurprising given that *in situ* NO_2^- oxidation kinetics studies are generally limited;
393 indeed, to our knowledge, there are only two studies from the coastal ocean (Olson 1981a; Zhang et al.
394 2020) and two from the Eastern Tropical North Pacific oxygen deficient zone (ETNP ODZ; with these
395 experiments conducted across a range of ambient oxygen concentrations; Sun et al., 2017, 2021). By
396 contrast, there exist numerous estimates of NO_2^- oxidation kinetic parameters determined using cultured
397 marine NOB (e.g., Sorokin et al., 2012; Nowka et al., 2015; Jacob et al., 2017; Kits et al., 2017; Zhang
398 et al., 2020). In general, culture experiments suggest far higher kinetic constants compared to the limited
399 *in situ* observations from the ocean, particularly for K_m (i.e., culture-based K_m estimates of 9-544 μM ;
400 Blackburne et al., 2007; Nowka et al., 2015; Ushiki et al., 2017).

401

402 The high K_m values derived for cultured NOB suggest that the affinity of these organisms for NO_2^- is
403 low. However, this is not what is observed in the environment, which indicates that the most abundant
404 marine NOB are not represented in the culture collection. For the Southern Ocean, we report high
405 substrate affinities of NOB, with K_m values ranging from 134 to 403 nM, which is largely within the
406 range documented for oxygenated coastal and open ocean waters (27-506 nM; Olson, 1981; Zhang et
407 al., 2020) (Table 2). In the low- to zero-oxygen waters of the ETNP ODZ, similarly low K_m values have
408 been reported (254 ± 161 nM; Sun et al., 2017), although values >5 μM have also been observed (Sun
409 et al., 2021), with these latter estimates associated with ambient NO_2^- concentrations >1 μM . We explore
410 the relationship between ambient NO_2^- concentration and K_m in detail in section 4.2 below. Our focus
411 is on the K_m values derived under conditions of low ambient NO_2^- (i.e., <250 nM) given that (some of)
412 the environmental factors affecting NO_2^- oxidation at high ambient NO_2^- concentrations appear to be
413 unique. For example, oxygen has been shown to decrease the rate of NO_2^- oxidation in the ODZs (Sun
414 et al., 2017, 2021) where novel clades of NOB have been detected (Sun et al., 2021). Additionally, NO_2^-
415 concentrations in the oxygenated open ocean seldom exceed 250 nM (Zakem et al., 2018), in contrast
416 to the ODZs (Bristow et al., 2016; Füssel et al., 2012).

417

418

419 Across our Southern Ocean transect, V_{max} ranged from 5 to 14 nM d^{-1} , which is relatively low compared
420 to estimates from other regions (Table 2), although such a comparison may not be particularly
421 informative as our rates (and typically those of others) are not normalized for NOB abundance. Our
422 V_{max} estimates are also low compared to a previous study of mixed-layer nitrification in the winter
423 Southern Ocean (Mdutyana et al., 2020). This difference may be partly due to the fact that the kinetics
424 experiments were conducted using surface (~ 7 m) seawater (and thus, the surface NOB community that
425 had been exposed to surface conditions, including elevated light), yet the highest rates of NO_2^- oxidation
426 typically occur near the base of the mixed layer, including in the Southern Ocean (Figure 3b-e; Sun et
427 al., 2017; Peng et al., 2018; Mdutyana et al., 2020). The opposite pattern has also been observed,
428 however (although not in the Southern Ocean), with deeper samples yielding a lower V_{max} than samples
429 collected in shallow waters (Sun et al., 2017; Zhang et al., 2020).

430

431 4.2 Environmental drivers of the NO_2^- oxidation kinetic parameters

432 We report maximum NO_2^- oxidation rates that generally increase towards the south and with decreasing
433 SST (recognizing that these parameters co-vary), although St 01 in the STZ and St 06 and 07 in the
434 MIZ deviate from this trend (Figure 4a and b; $R^2 = 0.019$; $p = 0.77$ and $R^2 = 0.12$; $p = 0.45$, respectively
435 when all the stations are considered and $R^2 = 0.92$; $p = 0.041$ and $R^2 = 0.94$; $p = 0.029$, respectively,
436 when St 01, 06, and 07 are excluded). It is possible that changes in the NOB community (composition
437 and/or abundance) across the transect explains some of the observed variability. Nonetheless, taking
438 latitude as a qualitative proxy for light, it is perhaps unsurprising that the maximum NO_2^- oxidation

439 rates increase southwards given that NOB are known to be at least partially light inhibited (Peng et al.,
440 2018; Ward, 2005; Olson, 1981b). This explanation does not hold for the stations in the MIZ, however,
441 at which V_{\max} decreases sharply despite these waters receiving the least light (less than 5 hours of weak
442 sunlight, versus ~ 7 hours at 55°S to ~ 9 hours at 37°S). The temperature at the MIZ stations was $<0^{\circ}\text{C}$,
443 which raises the possibility of a temperature effect on V_{\max} . Indeed, we previously observed a strong
444 decline in the V_{\max} associated with NH_4^+ oxidation at SSTs $<0^{\circ}\text{C}$ in the Southern Ocean, while at SSTs
445 ranging from 0.6°C to 16°C , V_{\max} was near invariant (Mdutyana et al., 2022).

446

447 Marine nitrification has been reported to be largely unaffected by temperature variations (Bianchi et al.,
448 1997; Horak et al., 2013; Baer et al., 2014), although NH_4^+ and NO_2^- oxidation may respond differently
449 to similar changes in temperature. For example, marine NOB incubated at temperatures ranging from
450 10°C to 35°C responded far more slowly to an increase in temperature than co-incubated AOA, resulting
451 in an accumulation of NO_2^- in the incubation bottles (Schaefer and Hollibaugh 2017). By contrast, we
452 previously observed no robust relationship between temperature and the maximum NH_4^+ oxidation rate
453 in the Southern Ocean (Mdutyana et al., 2022), a finding that is consistent with studies of NH_4^+
454 oxidation in the Arctic and temperate coastal ocean (Horak et al., 2013; Baer et al., 2014). Far less work
455 has been done to assess the response of NOB to temperature changes. In the absence of experiments
456 specifically designed to test the response of Southern Ocean NOB to temperature, it is difficult to
457 disentangle the effect(s) on NO_2^- oxidation of temperature *versus* light (and possibly other parameters
458 that co-vary with latitude, such as NO_2^- and/or micronutrient availability).

459

460 Plotting V_{\max} as a function of the ambient substrate concentration ($[\text{NO}_2^-]_{\text{amb}}$) reveals a strong positive
461 relationship for all but the MIZ stations (Figure 4c; $R^2 = 0.73$; $p = 0.065$ if the MIZ stations are
462 excluded). In particular, the STZ station (St 01), which appeared anomalous in the plots of V_{\max} versus
463 latitude and SST, is consistent with the other non-MIZ stations when evaluated in V_{\max} versus $[\text{NO}_2^-]_{\text{amb}}$
464 space. The positive relationship of V_{\max} to $[\text{NO}_2^-]_{\text{amb}}$ could be taken as evidence that NO_2^- availability
465 strongly controls the maximum achievable rate of NO_2^- oxidation. However, V_{\max} varies four-fold
466 across the transect while $[\text{NO}_2^-]_{\text{amb}}$ only changes by a factor of two, and $[\text{NO}_2^-]_{\text{amb}}$ is also correlated with
467 latitude ($R^2 = 0.51$, $p < 0.001$ for all surface $[\text{NO}_2^-]_{\text{amb}}$ data; Figure S2). Additionally, previous
468 wintertime Southern Ocean NO_2^- oxidation rates (albeit not V_{\max}) showed no relationship with ambient
469 NO_2^- concentration (Bianchi et al. 1997; Mdutyana et al. 2020). The extent to which V_{\max} is directly
470 controlled by $[\text{NO}_2^-]_{\text{amb}}$ is thus unclear, and it is likely that NOB community composition, light
471 availability, and temperature also play a role, with SST perhaps becoming more important at very low
472 temperatures (i.e., in the MIZ).

473

474 Our estimates of K_m reveal that NOB in the wintertime Southern Ocean have a high affinity for NO_2^-
475 that appears to decrease (i.e., the K_m rises) at higher latitudes (i.e., lower light) and lower temperatures,

476 with St 01 in the STZ again emerging as an exception (Figure 4d and e; $R^2 = 0.86$, $p = 0.008$ and $R^2 =$
477 0.86 , $p = 0.008$, respectively). Plotting our K_m values as a function of $[\text{NO}_2^-]_{\text{amb}}$ reveals a strong positive
478 relationship (Figure 4f; $R^2 = 0.83$, $p = 0.004$; black data points), implying that NO_2^- availability rather
479 than temperature or light exerts the dominant control on K_m . This trend further suggests that NOB are
480 well-adapted to the environment (or Southern Ocean region) in which they are found. Southern Ocean
481 mixed-layer NO_2^- concentrations are almost never <150 nM, regardless of the season (Fripiat et al.
482 2019; Mduyana et al. 2020; Zakem et al. 2018), yet the relationship of K_m to $[\text{NO}_2^-]_{\text{amb}}$ also holds at far
483 lower NO_2^- concentrations. The coloured data points in Figure 4f show K_m versus $[\text{NO}_2^-]_{\text{amb}}$ for four
484 additional regions where a Michaelis-Menten relationship of NO_2^- oxidation rate to NO_2^- concentration
485 was observed and where $[\text{NO}_2^-]_{\text{amb}}$ was <250 nM (two coastal ocean sites, the South China Sea (SCS;
486 Zhang et al., 2020) and Southern California Bight (SCB; Olson, 1981); one oligotrophic ocean site, the
487 subtropical South Atlantic (SSA; Fawcett et al. unpubl.); and two stations from the ETNP ODZ, where
488 oxygen concentrations ranged from 0 μM to 16.8 μM (Sun et al., 2017)). The robust positive relationship
489 of K_m to $[\text{NO}_2^-]_{\text{amb}}$ that emerges when these previous results are combined with our Southern Ocean
490 data ($R^2 = 0.68$, $p < 0.001$) strongly implicates $[\text{NO}_2^-]_{\text{amb}}$ as the dominant control on the K_m of NO_2^-
491 oxidation in the ocean, particularly at low $[\text{NO}_2^-]_{\text{amb}}$ (i.e., <250 nM).

492

493

494 The production of NO_2^- from NH_4^+ oxidation has recently been hypothesized to be vulnerable to iron
495 limitation (Mduyana et al., 2022) since AOB rely on iron-rich *cytochrome c* proteins (Arp et al., 2002;
496 Walker et al., 2010) and some AOA appear to have a low affinity for inorganic iron (Shafiee et al.
497 2019). NOB also contain iron-rich enzymes, such as nitrite oxidoreductase, which is responsible for
498 converting NO_2^- to NO_3^- (Meincke et al., 1992; Spieck et al., 1998). While we have no iron data with
499 which to compare our kinetic parameters, dissolved iron concentrations ($[\text{DFe}]$) were measured
500 throughout the euphotic zone at the depth-profile stations (St 08 to St 11; Mduyana et al., 2022). The
501 revised NO_2^- oxidation rates at these stations are weakly positively correlated with $[\text{DFe}]$ ($R^2 = 0.35$, p
502 $= 0.016$; Figure 5), indicating a potential role for iron in controlling NO_2^- oxidation. Combined with the
503 evidence that iron may also constrain marine NH_4^+ oxidation (Shafiee et al., 2019), this observation
504 implies that mixed-layer nitrification in the Southern Ocean may be iron-limited. Since phytoplankton
505 consumption of regenerated NO_3^- yields no net removal of atmospheric CO_2 in a mass balance sense
506 (Dugdale and Goering 1967; Yool et al., 2007), an iron-related control on mixed-layer nitrification
507 would help to limit the extent to which this process can weaken the Southern Ocean's biological pump
508 and would lead to enhanced competition between phytoplankton and nitrifiers for iron.

509

510 4.3 The persistence of elevated NO_2^- concentrations throughout the Southern Ocean's mixed layer

511 While still limited, there is growing evidence that marine AOA have a very high affinity for NH_4^+ (more
512 correctly, ammonia (NH_3), the substrate for NH_4^+ oxidation; Mduyana et al., 2022; Martens-Habbena
513 et al., 2009; Horak et al., 2013; Newell et al., 2013; Peng et al., 2016). Marine NOB also appear able to
514 access low concentrations of substrate, based on the few *in situ* studies conducted to-date, including
515 this one (Figure 4f; Olson, 1981; Sun et al., 2017; Zhang et al., 2020). This high substrate affinity is
516 perhaps unsurprising given that NO_2^- concentrations are generally near-zero throughout the oxygenated
517 ocean, rising modestly to values typically <500 nM at the PNM in (sub)tropical waters (Lomas and
518 Lipschultz 2006; Zakem et al. 2018) and <400 nM over the mixed layer in (sub)polar regions (Zakem
519 et al., 2018). The average surface NO_2^- concentration measured during Leg 1 of our cruise was $168 \pm$
520 48 nM (Figure 1a) and the average mixed-layer concentration for Leg 2 was 137 ± 57 nM (Figures 1b
521 and 3a). Similar concentrations have been observed previously across the Southern Ocean, including in
522 other seasons (Cavagna et al., 2015; Fripiat et al., 2019; Mduyana et al., 2020). Thus, while NO_2^-
523 oxidation in Southern Ocean surface waters is characterized by a low K_m , the affinity of NOB for NO_2^-
524 is apparently not high enough to completely remove the available NO_2^- .

525

526 The persistence of elevated NO_2^- concentrations in the mixed layer at high latitudes has previously been
527 attributed to the inability of iron- and/or light-limited phytoplankton to fully consume NO_2^- transported
528 to the surface with NO_3^- during deep mixing events (Zakem et al. 2018). However, subsurface NO_2^-
529 concentrations in the Southern Ocean are typically below detection (Figure 1b and 3a; Olsen et al.,
530 2016), so it is unclear how deep mixing could supply measurable NO_2^- to the euphotic zone. We thus
531 discount subsurface mixing as a primary explanation for the elevated Southern Ocean mixed-layer NO_2^-
532 concentrations, as were observed during our study and in other seasons (e.g., Fripiat et al., 2019).

533

534

535 A second possible source of elevated mixed-layer NO_2^- is efflux following partial NO_3^- reduction to
536 NO_2^- by phytoplankton (Lomas and Lipschultz 2006), which has been extensively documented in
537 laboratory and field studies (see Collos, 1998 for a review). The release of NO_2^- by phytoplankton is
538 hypothesized to result from light limitation of intracellular NO_2^- reduction (Vaccaro and Ryther 1960;
539 Kiefer, Olson, and Holm-Hansen 1976), short-term increases in irradiance to which phytoplankton
540 cannot adapt (Lomas and Lipschultz 2006), iron limitation of NO_3^- assimilation (Milligan and Harrison
541 2000), and/or release of phytoplankton from NO_3^- limitation following a period of starvation (Sciandra
542 and Amara 1994). While some of these mechanisms may be ongoing in the Southern Ocean, they all
543 require the initial uptake of NO_3^- by phytoplankton. This process occurs in the winter mixed layer at
544 rates that are too low to support NO_2^- efflux to the extent that it would allow NO_2^- to accumulate to
545 concentrations of 100-400 nM (Figure S3; Philibert et al., 2015; Mduyana et al., 2020) while
546 simultaneously being removed by NO_2^- oxidation. Additionally, we observe a reasonable correlation

547 between the NH_4^+ oxidation rates and the ambient NO_2^- concentration ($R^2 = 0.46$, $p < 0.001$; Figure S4),
548 which implies that NO_2^- derives mainly from NH_4^+ oxidation rather than phytoplankton efflux.

549

550 A third potential explanation for elevated mixed-layer NO_2^- is a decoupling of NH_4^+ and NO_2^- oxidation,
551 which appears to be widespread in the environment (e.g., Ward and Zafiriou, 1988; Beman et al., 2013).
552 In the oxygenated ocean, NH_4^+ oxidation has been considered the rate-limiting step in the nitrification
553 pathway because NO_2^- seldom accumulates in the mixed layer (Kendall 1998; Kowalchuk and Stephen
554 2001; Walker et al. 2010; Vajjala et al. 2013). However, rate measurements from numerous ocean
555 regions show contrasting results, with NO_2^- oxidation sometimes outpacing NH_4^+ oxidation (Peng et al.
556 2018; Dore and Karl 1996; Bristow et al. 2015; Horrigan et al. 1990) while in other cases, NH_4^+
557 oxidation is dominant (Ward and Kilpatrick 1991; Kalvelage et al. 2013; Clark et al. 2008). The limited
558 data available from previous Southern Ocean investigations show no clear trend (Bianchi et al., 1997;
559 Mduyana et al., 2020). In the present study, mixed-layer $\text{corrNO}_2^-_{\text{ox}}$ rates are two- to seven-times lower
560 than the coincidentally measured $\text{corrNH}_4^+_{\text{ox}}$ (Figures 3 and 6). Additionally, the maximum rates of
561 NO_2^- oxidation (V_{max}) that we measure in this study for the surface NOB community (~ 5 to 13 nM d^{-1} ;
562 Figure 2) are on average half those determined at the same stations for NH_4^+ oxidation (14 to 23 nM d^{-1} ;
563 Mduyana et al., 2022). At the time of our sampling, therefore, NO_2^- oxidation was rate-limiting for
564 nitrification, which likely accounts for much of the NO_2^- accumulated in the Southern Ocean's winter
565 mixed layer .

566

567 If a decoupling of NH_4^+ and NO_2^- oxidation is predominantly responsible for NO_2^- accumulation, an
568 obvious question is why these rates are not balanced. Environmental factors like temperature and light
569 may play a role (Ward, 2008), as may iron limitation and the different ecophysiologicals of NH_4^+ and
570 NO_2^- oxidizers. AOA have been shown to adapt more rapidly than NOB to a change in temperature
571 (Schaefer and Hollibaugh, 2017); however, seasonal SST changes within the various zones of the
572 Southern Ocean are fairly small and the aforementioned study showing the differential thermal response
573 of AOA and NOB was conducted at higher temperatures than those experienced in much of the Southern
574 Ocean. With regards to light, there is evidence from culture and field studies that NOB are more
575 photosensitive than AOA and AOB (Bock, 1965; Olson, 1981b; Qin et al., 2014). Our data are
576 consistent with this notion insofar as the V_{max} associated with NO_2^- oxidation in surface waters rises
577 with increasing latitude (and thus decreasing light; Figure 4a) while the V_{max} derived for NH_4^+ oxidation
578 remains largely unchanged across >30 degrees of latitude (Mduyana et al., 2022). However, the
579 ambient NO_2^- concentration in Southern Ocean surface waters rises near linearly with latitude (Figure
580 S2a) while the NH_4^+ concentration resembles a step function, increasing from $\sim 100 \text{ nM}$ north of the
581 SAF to $\sim 700 \text{ nM}$ south of the SAF, over a distance of roughly one degree of latitude (Figure S2b). The
582 differing trends in V_{max} may thus have more to do with substrate availability than photoinhibition.

583

584 Mixing, particularly deep winter overturning, might also contribute to a decoupling of NH_4^+ and NO_2^-
585 oxidation. In coastal waters, deep winter mixing has been shown to dilute the nitrifier community, with
586 AOO subsequently observed to recover more rapidly than NOB. This differential rate of recovery has
587 been hypothesized to result in a period of low rates of NO_2^- oxidation during which the co-occurring
588 NH_4^+ oxidation rates remain elevated, ultimately causing NO_2^- to accumulate in the surface layer (Haas
589 et al., 2021). While a similar effect may play a role in NO_2^- accumulation in the open Southern Ocean,
590 it is unlikely that the entire NO_2^- reservoir can be attributed to this process. The rates of NH_4^+ oxidation
591 are only slightly higher than the NO_2^- oxidation rates in the winter mixed layer (Figure 3) and the mixed-
592 layer NH_4^+ concentrations are elevated (Figure 3f). These observations imply that NH_4^+ oxidizers are
593 limited by something other than NH_4^+ substrate,). These observations then from catalysing higher rates
594 of NO_2^- production (and thus NO_2^- accumulation).

595
596 Nitrite oxidoreductase (NXR), the enzyme possessed by NOB that is responsible for aerobic NO_2^-
597 oxidation to NO_3^- , is an iron-sulfur molybdoprotein (Sundermeyer-Klinger et al. 1984; Meincke et al.
598 1992; Lückner et al. 2010). As such, NO_2^- oxidation has a significant iron requirement (Saito et al., 2020;
599 Bayer et al., 2021), intimated by the relationship we observe between $\text{corrNO}_2^-_{\text{ox}}$ and DFe (Figure 5).
600 Additionally, NO_2^- accumulation at the PNM in the California Current has been hypothesized to be
601 caused by iron limitation of NOB (Santoro et al. 2013). AOB also require iron, in particular for the
602 oxidation of hydroxylamine, which is catalyzed by the heme-rich hydroxylamine oxidoreductase
603 complex (Arp et al., 2002; Walker et al., 2010). By contrast, AOA, the dominant marine NH_4^+ oxidizers,
604 rely mainly on copper-containing proteins to mediate NH_4^+ oxidation (Amin et al., 2013; Walker et al.,
605 2010; Santoro et al., 2015). In the iron-limited Southern Ocean, it is thus possible that iron scarcity
606 more strongly limits NO_2^- than NH_4^+ oxidation. However, recent culture and proteomic work suggests
607 that some AOA may actually have a high iron requirement (Alyson E. Santoro et al. 2015; Carini,
608 Dupont, and Santoro 2018; Qin et al. 2018; Shafiee et al. 2019), and we have previously hypothesized
609 an iron-related control on NH_4^+ oxidation in the Southern Ocean (Mdutyana et al., 2022). Deeper
610 investigation is thus required to characterize the role of iron in controlling the relative rates of NH_4^+ and
611 NO_2^- oxidation, and the implications for the complete nitrification pathway.

612
613 A further consideration is differences in the ecology of AOA and NOB. Marine NOB are an order of
614 magnitude less abundant than AOA (e.g., Füssel et al., 2012; Beman et al., 2013b; Pachiadaki et al.,
615 2017; Damashek et al., 2019; Kitzinger et al., 2020) and roughly three-times larger (Watson and
616 Waterbury, 1971; Könneke et al., 2005; Martens-Habbena et al., 2009; Pachiadaki et al., 2017). While
617 marine NOB appear to have a high affinity for ambient NO_2^- , the *in situ* K_m values derived to-date are
618 not as low as those reported for NH_4^+ oxidation (Horak et al., 2013; Peng et al., 2016; Xu et al., 2019;
619 Zhang et al., 2020; Mdutyana et al. 2022), which is perhaps to be expected given the larger size of
620 NOB versus AOA. Resource limitation theory posits that nitrifiers (NOB and AOA) require a

621 subsistence concentration of substrate (R^*) to maintain their population, and that those with the lowest
622 R^* will outcompete all other organisms limited by the same resource, provided that their V_{\max} is higher
623 than their loss rate due to grazing and/or viral lysis (Zakem et al., 2018). Because NOB are larger than
624 AOA, they will have a higher R^* even before grazing pressure is factored in. Their larger size also
625 means that NOB are more likely to be grazed than AOA, which will further increase their R^* , as will
626 the fact that their maximum growth rates are low and thus vulnerable to being outpaced by their loss
627 rate. Taken together, these factors will increase R^* , potentially resulting in the accumulation of NO_2^- in
628 the water column, and may help to explain why the K_m for NO_2^- oxidation, in the Southern Ocean and
629 elsewhere, is considerably higher than the K_m derived for NH_4^+ oxidation. Additionally, the fact that
630 NOB will be preferentially grazed over AOA may contribute to NO_2^- oxidation being rate-limiting for
631 nitrification.

632

633 That NO_2^- oxidation was rate-limiting at the time of our sampling does not necessarily explain the
634 accumulation of NO_2^- in the Southern Ocean mixed layer year-round. Neither NH_4^+ nor NO_2^- oxidation
635 occur at elevated rates in summer or autumn (Bianchi et al., 1997; Mduyana et al., 2020), yet the
636 elevated NO_2^- concentrations persist during these seasons (Cavagna et al., 2015; Fripiat et al., 2019;
637 Mduyana et al., 2020). To fit a Michaelis-Menten function to our experimental data required amending
638 the classical equation (equation 2) to allow for a positive x-intercept (i.e., a non-zero S value at which
639 V was still zero, the C parameter in equation 3) (Archontoulis and Miguez, 2014). Additionally, at most
640 stations, the NO_2^- oxidation rates did not increase substantially following the initial two or three
641 substrate amendments (i.e., in Figure 2, the slope of the relationship between V and S is less steep for
642 the initial two to three values of S than at higher S values). Practically, our findings suggest that
643 Southern Ocean NOB require a minimum (i.e., “threshold”) NO_2^- concentration below which the NO_2^-
644 concentration becomes severely limiting. Coupled with weak NO_2^- drawdown by iron- and/or light-
645 limited phytoplankton during their incomplete consumption of the $\text{NO}_3^- + \text{NO}_2^-$ pool, a threshold
646 substrate requirement of NOB can explain the year-round persistence of non-zero mixed-layer NO_2^-
647 since it implies that there is no mechanism by which NO_2^- can be completely exhausted.

648

649 The existence of a NO_2^- concentration threshold may indicate limitation of the membrane-bound NXR
650 enzyme, either by NO_2^- or by another essential nutrient. Recently, using NXR concentrations, estimates
651 of NXR specific activity, and direct measurements of *in situ* NO_2^- oxidation rates, Saito et al., (2020)
652 deduced that *Nitrospina* NXR is undersaturated with NO_2^- in the tropical Pacific, possibly due to iron
653 limitation. The authors suggest that under iron-scarce conditions, it becomes increasingly difficult for
654 NOB to synthesize NXR and thus to oxidize NO_2^- . A similar dynamic may be at play in the Southern
655 Ocean, with limited synthesis of NXR at low iron concentrations resulting in a decrease in the efficiency
656 of the NO_2^- oxidation pathway that manifests most strongly when the ambient NO_2^- concentration is
657 also low. This inefficiency could be alleviated at higher NO_2^- concentrations since NOB (even with a

658 paucity of NXR) are less likely to experience diffusion limitation with respect to NO_2^- when there is
659 more of this substrate available (Pasciak and Gavis 1974). Regardless of its mechanistic basis, limitation
660 of NOB NXR would help to explain the perennially high concentrations of NO_2^- in the Southern Ocean
661 mixed layer. Moreover, environmental factors unique to the Southern Ocean, such as limited iron
662 availability, may be instrumental in setting the NO_2^- threshold and associated elevated mixed-layer NO_2^-
663 concentrations.

664

665 Our observations raise the question of why a similar NO_2^- concentration threshold has not been reported
666 for other ocean regions, particularly those characterized by similar conditions to the Southern Ocean.
667 This may partly be due to the very limited number of NO_2^- oxidation kinetics experiments that have
668 been conducted in the open ocean and/or to the fact that a classic Michaelis-Menten function is usually
669 imposed upon kinetics data, with V assumed to increase as soon as $S > 0$. Additionally, depending on
670 the maximum substrate concentration added during kinetics experiments (i.e., the maximum
671 concentration on the x-axis of the V versus S plot), it can be difficult to discern a possible threshold
672 NO_2^- concentration by simply examining the plots. Inspection of published Michaelis-Menten curves
673 does reveal the possibility of a non-zero C value in some cases, including in the ETNP ODZ (Sun et al.,
674 2021) and associated with the PNM in the South China Sea (Zhang et al., 2020). However, there are
675 also published curves that clearly intercept the origin in V versus S space (Olson, 1981a; Sun et al.,
676 2017), underscoring the need for further investigation of the conditions that lead to a threshold NO_2^-
677 concentration requirement of NOB.

678

679 **5. Concluding remarks**

680 In this study, we present the first NO_2^- oxidation kinetic constants for the Southern Ocean, derived from
681 surface experiments conducted during winter 2017. All the experiments were well-described by the
682 Michaelis-Menten equation, provided that a location parameter, C , was included in the model. V_{\max}
683 ranged from 5.2 ± 0.1 to 13 ± 0.4 nM d^{-1} and K_m ranged from 134 ± 8 to 403 ± 24 nM , with the latter
684 parameter showing a strong positive relationship with the ambient NO_2^- concentration. We interpret the
685 positive values of C (range of 115 ± 2.3 to 245 ± 18 nM) to indicate an ambient NO_2^- concentration
686 threshold below which NOB, and thus NO_2^- oxidation, are impeded. We hypothesize that this threshold
687 indicates substrate limitation of NXR, possibly exacerbated by the low ambient iron concentrations
688 characteristic of the upper Southern Ocean. Our kinetics experiments were conducted in surface waters
689 only, which raises the question of the relevance of our findings for deeper euphotic zone waters. For
690 instance, it is possible that surface nitrifier communities may be more iron limited than those living
691 nearer the base of the euphotic zone. However, in the winter Southern Ocean, the euphotic zone is
692 always considerably shallower than the mixed layer (50-75 m versus 100-250 m) such that both layers
693 are typically very well-mixed, as is apparent from the near-invariant mixed-layer (and thus euphotic-

694 zone) distributions of nutrients (Fig 1b-c), including trace metals (Cloete et al., 2019). One might
695 therefore expect the nitrifiers to also be evenly distributed over the euphotic zone and mixed layer. The
696 light flux will not be homogenous over these layers, however. Indeed, light availability is frequently
697 invoked to explain the vertical distribution of nitrification rates because nitrifier activity is impeded at
698 high light (Horrigan et al., 1981; Olson, 1981b; Qin et al., 2014; Peng et al., 2018). Our nitrification
699 depth profiles do not show a vertical trend, instead remaining similar throughout the euphotic zone and
700 only rising near the base of the mixed layer (Figure 3b-e). We thus consider the results of our surface
701 kinetics experiments to be broadly applicable to the euphotic zone in winter. From the depth-profile
702 measurements, we deduce that the rate-limiting step for mixed-layer nitrification in the winter Southern
703 Ocean is NO_2^- oxidation. Despite this, NO_3^- production from NO_2^- oxidation accounted for 63-237% of
704 the NO_3^- consumed by phytoplankton, consistent with previous wintertime observations from the
705 Atlantic sector (Mdutyana et al., 2020). The implication of this finding is that most of the mixed-layer
706 NO_3^- consumed by phytoplankton in winter, and likely also a significant fraction assimilated in spring,
707 supports regenerated rather than new production (Yool et al., 2007; Mdutyana et al., 2020).

708

709 NO_2^- oxidation, as the ultimate pathway connecting reduced N to its most oxidized form (NO_3^-), is
710 important throughout the water column, but particularly in the upper layer where the supply of reduced
711 N is highest. The production of NO_3^- within the mixed layer from *in situ* nitrification can complicate
712 the application of the new production paradigm as a framework for estimating carbon export potential,
713 which advocates for additional measurements of this pathway over the upper ~200 m. Additionally, it
714 is becoming increasingly clear that we lack a mechanistic understanding of the controls on nitrification
715 (both NH_4^+ and NO_2^- oxidation), which renders it challenging to model both its magnitude and
716 distribution, as well as to assess how these may change in future. In particular, further study of the role
717 of iron in controlling nitrification is required, particularly in the Southern Ocean where the mixed
718 layer's biological N cycle is dominated by nitrification in winter (Smart et al., 2015; Mdutyana et al.,
719 2020) and surface-layer iron remains scarce throughout the year (Tagliabue et al., 2012).

720

721 **Data availability**

722 All data used in this manuscript can be found at DIO: 10.5281/zenodo.6791408

723

724 **Author contribution**

725 MM and SEF planned the campaign; MM and JMB collected the samples and conducted the
726 experiments; MM and XS made the measurements, with support from BBW; MM, TM, and SEF
727 analysed the data; MM and SEF wrote the manuscript draft, with substantial input from BBW and TM;
728 All authors reviewed, edited, and approved the manuscript.

729

730 **Competing interests**

731 The authors declare that they have no conflict of interest.

732

733

734 **Acknowledgements**

735 We thank Captain Knowledge Bengu and the crew of the R/V *S.A. Agulhas II* and Chief Scientist M.
736 Vichi for professional support during the cruise, as well as the Marine Biogeochemistry Lab team at the
737 University of Cape Town (UCT), C. Karriem for extensive administrative support, and I. Newton and
738 J. Luyt at the UCT Stable Light Isotope Laboratory for filter analyses. The nitrification measurements
739 were made possible through the Princeton University Visiting Student Research Collaborator program-
740 we are especially grateful to S. Oleynik in the Department of Geosciences for his expert assistance
741 during the first author's visit. This work was supported by the South African National Research
742 Foundation through Antarctic Programme grants to S.E.F. (110735, 129232), and S.J.T. (93076), and
743 postgraduate scholarships to M.M. (112380), T.M. (114673 and 130826) and J.M.B. (110732); by UCT
744 through a Harry Crossley Foundation Research Fellowship to M.M., postgraduate scholarship to T.M.,
745 Vice-Chancellor (VC) Research Scholarships to J.M.B., a VC Future Leaders 2030 award to S.E.F.,
746 and a Research Committee Equipment grant to S.E.F.; by the African Academy of Sciences/Royal
747 Society through a FLAIR Fellowship to S.E.F; and by US National Science Foundation grants to
748 B.B.W. The authors also acknowledge the South African Department of Science and Innovation's
749 Biogeochemistry Research Infrastructure Platform.

750

751

752

753 **References**

- 754 Amin, Shady A., James W. Moffett, Willm Martens-Habbena, Jeremy E. Jacquot, Yang Han, Allan
 755 Devol, Anitra E. Ingalls, David A. Stahl, and E. Virginia Armbrust. 2013. “Copper
 756 Requirements of the Ammonia-Oxidizing Archaeon *Nitrosopumilus Maritimus* SCM1 and
 757 Implications for Nitrification in the Marine Environment.” *Limnology and Oceanography* 58 (6):
 758 2037–45. <https://doi.org/10.4319/lo.2013.58.6.2037>.
- 759 Archontoulis, Sotirios V., and Fernando E. Miguez. 2014. “Nonlinear Regression Models and
 760 Applications in Agricultural Research.” *Agronomy Journal* 107 (2): 786–98.
 761 <https://doi.org/10.2134/agronj2012.0506>.
- 762 Arp, Daniel J., Luis A. Sayavedra-Soto, and Norman G. Hommes. 2002. “Molecular Biology and
 763 Biochemistry of Ammonia Oxidation by *Nitrosomonas Europaea*.” *Archives of Microbiology*
 764 178 (4): 250–55. <https://doi.org/10.1007/s00203-002-0452-0>.
- 765 Baer, S. E., T. L. Connelly, R. E. Sipler, P. L. Yager, and D. A. Bronk. 2014. “Effect of Temperature
 766 on Rates of Ammonium Uptake and Nitrification in the Western Coastal Arctic during Winter,
 767 Spring, and Summer.” *Global Biogeochemical Cycles* 28: 1455–66.
 768 <https://doi.org/10.1111/1462-2920.13280>.
- 769 Bayer, Barbara, Mak A. Saito, Matthew R. McIlvin, Sebastian Lucker, Dawn M. Moran, Thomas S.
 770 Lankiewicz, Christopher L. Dupont, and Alyson E. Santoro. 2021. “Metabolic Versatility of the
 771 Nitrite-Oxidizing Bacterium *Nitrospira Marina* and Its Proteomic Response to Oxygen-Limited
 772 Conditions.” *ISME Journal* 15 (4): 1025–39. <https://doi.org/10.1038/s41396-020-00828-3>.
- 773 Belkin, Igor M., and Arnold L. Gordon. 1996. “Southern Ocean Fronts from the Greenwich Meridian
 774 to Tasmania.” *Journal of Geophysical Research C: Oceans*. <https://doi.org/10.1029/95JC02750>.
- 775 Beman, J. Michael, Joy Leilei Shih, and Brian N. Popp. 2013. “Nitrite Oxidation in the Upper Water
 776 Column and Oxygen Minimum Zone of the Eastern Tropical North Pacific Ocean.” *ISME*
 777 *Journal* 7 (11): 2192–2205. <https://doi.org/10.1038/ismej.2013.96>.
- 778 Beman, J. Michael, Brian N. Popp, and Christopher A. Francis. 2008. “Molecular and
 779 Biogeochemical Evidence for Ammonia Oxidation by Marine Crenarchaeota in the Gulf of
 780 California.” *ISME Journal* 2 (4): 429–41. <https://doi.org/10.1038/ismej.2007.118>.
- 781 Bianchi, Micheline, F. Feliatra, Paul Tréguer, Marie Anne Vincendeau, and Jean Morvan. 1997.
 782 “Nitrification Rates, Ammonium and Nitrate Distribution in Upper Layers of the Water Column
 783 and in Sediments of the Indian Sector of the Southern Ocean.” *Deep-Sea Research Part II:*
 784 *Topical Studies in Oceanography* 44 (5): 1017–32. [https://doi.org/10.1016/S0967-](https://doi.org/10.1016/S0967-0645(96)00109-9)
 785 [0645\(96\)00109-9](https://doi.org/10.1016/S0967-0645(96)00109-9).
- 786 Birch, Colin P.D. 1999. “A New Generalized Logistic Sigmoid Growth Equation Compared with the
 787 Richards Growth Equation.” *Annals of Botany* 83 (6): 713–23.
 788 <https://doi.org/10.1006/anbo.1999.0877>.
- 789 Blackburne, Richard, Vel M Vadivelu, and Zhiguo Yuan. 2007. “Kinetic Characterisation of an
 790 Enriched *Nitrospira* Culture with Comparison to *Nitrobacter*” 41: 3033–42.
 791 <https://doi.org/10.1016/j.watres.2007.01.043>.
- 792 Bock, Eberhard. 1965. “Vergleichende Untersuchungen Über Die Wirkung Sichtbaren Lichtes Auf
 793 *Nitrosomonas Europaea* Und *Nitrobacter Winogradskyi*.” *Archiv Für Mikrobiologie*.
 794 <https://doi.org/10.1007/BF00406848>.
- 795 Bristow, Laura A., Tage Dalsgaard, Laura Tiano, Daniel B. Mills, Anthony D. Bertagnolli, Jody J.
 796 Wright, Steven J. Hallam, et al. 2016. “Ammonium and Nitrite Oxidation at Nanomolar Oxygen
 797 Concentrations in Oxygen Minimum Zone Waters.” *Proceedings of the National Academy of*
 798 *Sciences* 113 (38): 10601–6. <https://doi.org/10.1073/pnas.1600359113>.

- 799 Bristow, Laura A., Neha Sarode, John Cartee, Alejandro Caro-Quintero, Bo Thamdrup, and Frank J.
800 Stewart. 2015. "Biogeochemical and Metagenomic Analysis of Nitrite Accumulation in the Gulf
801 of Mexico Hypoxic Zone." *Limnology and Oceanography* 60 (5): 1733–50.
802 <https://doi.org/10.1002/lno.10130>.
- 803 Caranto, Jonathan D., and Kyle M. Lancaster. 2017. "Nitric Oxide Is an Obligate Bacterial
804 Nitrification Intermediate Produced by Hydroxylamine Oxidoreductase." *Proceedings of the
805 National Academy of Sciences of the United States of America* 114 (31): 8217–22.
806 <https://doi.org/10.1073/pnas.1704504114>.
- 807 Carini, Paul, Christopher L. Dupont, and Alyson E. Santoro. 2018. "Patterns of Thaumarchaeal Gene
808 Expression in Culture and Diverse Marine Environments." *Environmental Microbiology* 20 (6):
809 2112–24. <https://doi.org/10.1111/1462-2920.14107>.
- 810 Carvalho, Filipa, Josh Kohut, Matthew J. Oliver, and Oscar Schofield. 2017. "Defining the
811 Ecologically Relevant Mixed-Layer Depth for Antarctica's Coastal Seas." *Geophysical
812 Research Letters*. <https://doi.org/10.1002/2016GL071205>.
- 813 Cavagna, A. J., F. Fripiat, M. Elskens, P. Mangion, L. Chirurgien, I. Closset, M. Lasbleiz, et al. 2015.
814 "Production Regime and Associated N Cycling in the Vicinity of Kerguelen Island, Southern
815 Ocean." *Biogeosciences* 12 (21): 6515–28. <https://doi.org/10.5194/bg-12-6515-2015>.
- 816 Clark, Darren R, Andrew P Rees, Ian Joint, Source Limnology, No Jan, Darren R Clark, Andrew P
817 Rees, and Ian Joint. 2008. "Ammonium Regeneration and Nitrification Rates in the Oligo
818 Trophic Atlantic Ocean : Implications for New Production Estimates." *Limnology and
819 Oceanography* 53 (1): 52–62.
- 820 Cloete, R., J. C. Loock, T. Mtshali, S. Fietz, and A. N. Roychoudhury. 2019. "Winter and Summer
821 Distributions of Copper, Zinc and Nickel along the International GEOTRACES Section
822 GIPY05: Insights into Deep Winter Mixing." *Chemical Geology* 511 (February 2018): 342–57.
823 <https://doi.org/10.1016/j.chemgeo.2018.10.023>.
- 824 Collos, Yves. 1998. "Nitrate Uptake, Nitrite Release and Uptake, and New Production Estimates."
825 *Marine Ecology Progress Series* 171: 293–301. <https://doi.org/10.3354/meps171293>.
- 826 Damashek, Julian, Bradley B. Tolar, Qian Liu, Aimee O. Okotie-Oyekan, Natalie J. Wallsgrove,
827 Brian N. Popp, and James T. Hollibaugh. 2019. "Microbial Oxidation of Nitrogen Supplied as
828 Selected Organic Nitrogen Compounds in the South Atlantic Bight." *Limnology and
829 Oceanography* 64 (3): 982–95. <https://doi.org/10.1002/lno.11089>.
- 830 DeVries, Tim, Mark Holzer, and Francois Primeau. 2017. "Recent Increase in Oceanic Carbon
831 Uptake Driven by Weaker Upper-Ocean Overturning." *Nature* 542 (7640): 215–18.
832 <https://doi.org/10.1038/nature21068>.
- 833 Diaz, Frédéric, and Patrick Raimbault. 2000. "Nitrogen Regeneration and Dissolved Organic Nitrogen
834 Release during Spring in a NW Mediterranean Coastal Zone (Gulf of Lions): Implications for
835 the Estimation of New Production." *Marine Ecology Progress Series* 197: 51–65.
836 <https://doi.org/10.3354/meps197051>.
- 837 DiFiore, Peter J., Daniel M. Sigman, and Robert B. Dunbar. 2009. "Upper Ocean Nitrogen Fluxes in
838 the Polar Antarctic Zone: Constraints from the Nitrogen and Oxygen Isotopes of Nitrate."
839 *Geochemistry, Geophysics, Geosystems* 10 (11). <https://doi.org/10.1029/2009GC002468>.
- 840 Dore, John E, and David A I Karl. 1996. "Nitrification in the Euphotic Zone as a Source for Nitrite ,
841 Nitrate , and Nitrous Oxide at Station ALOHA" 41: 1619–28.
- 842 Dugdale, R. C., and J. J. Goering. 1967. "Uptake of New and Regenerated Forms of Nitrogen in
843 Primary Productivity." *Limnology and Oceanography* 12 (2): 196–206.
844 <https://doi.org/10.4319/lo.1967.12.2.0196>.

- 845 Dugdale, R C, and F P Wilkerson. 1986. "The Use of N-15 To Measure Nitrogen Uptake in Eutrophic
846 Oceans - Experimental Considerations." *Limnology and Oceanography* 31 (4): 673–89.
- 847 Eppley, Richard W., and Bruce J. Peterson. 1979. "Particulate Organic Matter Flux and Planktonic
848 New Production in the Deep Ocean." *Nature* 282 (5740): 677–80.
849 <https://doi.org/10.1038/282677a0>.
- 850 Fripiat, François, Anja S. Studer, Gerald H. Haug, Sergey Oleynik, Alfredo Martínez-García, Sandi
851 M. Smart, Florian Rubach, Daniel M. Sigman, Sarah E. Fawcett, and Preston C. Kemeny. 2019.
852 "The Isotope Effect of Nitrate Assimilation in the Antarctic Zone: Improved Estimates and
853 Paleoceanographic Implications." *Geochimica et Cosmochimica Acta* 247: 261–79.
854 <https://doi.org/10.1016/j.gca.2018.12.003>.
- 855 Füssel, Jessika, Phyllis Lam, Gaute Lavik, Marlene M. Jensen, Moritz Holtappels, Marcel Günter, and
856 Marcel M.M. Kuypers. 2012. "Nitrite Oxidation in the Namibian Oxygen Minimum Zone." *ISME Journal* 6 (6): 1200–1209. <https://doi.org/10.1038/ismej.2011.178>.
- 858 Glibert, Patricia M., Mark R. Dennett, and Joel C. Goldman. 1985. "Inorganic Carbon Uptake by
859 Phytoplankton in Vineyard Sound, Massachusetts. II. Comparative Primary Productivity and
860 Nutritional Status of Winter and Summer Assemblages." *Journal of Experimental Marine
861 Biology and Ecology* 86 (2). [https://doi.org/10.1016/0022-0981\(85\)90025-5](https://doi.org/10.1016/0022-0981(85)90025-5).
- 862 Glibert, Patricia M., Fredric Lipschultz, James J. Mccarthy, and Mark A. Altabet. 1982. "Isotope
863 Dilution Models of Uptake and Remineralization of Ammonium By Marine Plankton."
864 *Limnology and Oceanography* 27 (4): 639–50. <https://doi.org/10.4319/lo.1982.27.4.0639>.
- 865 Grasshoff K, Ehrhardt M, and, Kremling K. 1983. *Methods of Seawater Analysis*. Verlag Chemie,
866 New York.
- 867 Gruber, Nicolas, Dominic Clement, Brendan R. Carter, Richard A. Feely, Steven van Heuven, Mario
868 Hoppema, Masao Ishii, et al. 2019. "The Oceanic Sink for Anthropogenic CO₂ from 1994 to
869 2007." *Science* 363 (6432): 1193–99. <https://doi.org/10.1126/science.aau5153>.
- 870 Haas, Sebastian, Brent M. Robicheau, Subhadeep Rakshit, Jennifer Tolman, Christopher K. Algar,
871 Julie LaRoche, and Douglas W.R. Wallace. 2021. "Physical Mixing in Coastal Waters Controls
872 and Decouples Nitrification via Biomass Dilution." *Proceedings of the National Academy of
873 Sciences of the United States of America* 118 (18). <https://doi.org/10.1073/pnas.2004877118>.
- 874 Hauck, J., C. Völker, D. A. Wolf-Gladrow, C. Laufkötter, M. Vogt, O. Aumont, L. Bopp, et al. 2015.
875 "On the Southern Ocean CO₂ Uptake and the Role of the Biological Carbon Pump in the 21st
876 Century." *Global Biogeochemical Cycles* 29 (9): 1451–70.
877 <https://doi.org/10.1002/2015GB005140>.
- 878 Heiss, Elise M., and Robinson W. Fulweiler. 2017. "Erratum to 'Coastal Water Column Ammonium
879 and Nitrite Oxidation Are Decoupled in Summer' (Estuarine, Coastal and Shelf Science (2016)
880 178 (110–119) (S0272771417301981) (10.1016/j.ecss.2017.02.023))." *Estuarine, Coastal and
881 Shelf Science* 193: 37–45. <https://doi.org/10.1016/j.ecss.2016.12.026>.
- 882 Holmes, R M, A Aminot, R Kerouel, B A Hooker, and B J Peterson. 1999. "A Simple and Precise
883 Method for Measuring Ammonium in Marine and Freshwater Ecosystems." *Canadian Journal
884 of Fisheries and Aquatic Sciences*. <https://doi.org/10.1139/cjfas-56-10-1801>.
- 885 Horak, Rachel E.A., Wei Qin, Andy J. Schauer, E. Virginia Armbrust, Anitra E. Ingalls, James W.
886 Moffett, David A. Stahl, and Allan H. Devol. 2013. "Ammonia Oxidation Kinetics and
887 Temperature Sensitivity of a Natural Marine Community Dominated by Archaea." *ISME
888 Journal* 7 (10): 2023–33. <https://doi.org/10.1038/ismej.2013.75>.
- 889 Horrigan, S. G., J. P. Montoya, J. L. Nevins, J. J. McCarthy, H. Ducklow, R. Goericke, and T.
890 Malone. 1990. "Nitrogenous Nutrient Transformations in the Spring and Fall in the Chesapeake

- 891 Bay.” *Estuarine, Coastal and Shelf Science* 30 (4). [https://doi.org/10.1016/0272-7714\(90\)90004-](https://doi.org/10.1016/0272-7714(90)90004-B)
892 B.
- 893 Jacob, Juliane, Boris Nowka, Véronique Merten, Tina Sanders, Eva Spieck, and Kirstin Dähnke.
894 2017. “Oxidation Kinetics and Inverse Isotope Effect of Marine Nitrite-Oxidizing Isolates.”
895 *Aquatic Microbial Ecology* 80 (3): 289–300. <https://doi.org/10.3354/ame01859>.
- 896 Jong, Ehlke de, Marcello Vichi, Carolin Birgitta Mehlmann, Clare Eayrs, Wade De Kock, Marcel
897 Moldenhauer, and Riesna Reuben Audh. 2018. “Sea Ice Conditions within the Antarctic
898 Marginal Ice Zone in Winter 2017, Onboard the SA Agulhas II.” *Pangaea*, 2018.
899 <https://doi.org/10.1594/PANGAEA.885211>.
- 900 Kalvelage, Tim, Gaute Lavik, Phyllis Lam, Sergio Contreras, Lionel Arteaga, Carolin R. Löscher,
901 Andreas Oschlies, Aurélien Paulmier, Lothar Stramma, and Marcel M.M. Kuypers. 2013.
902 “Nitrogen Cycling Driven by Organic Matter Export in the South Pacific Oxygen Minimum
903 Zone.” *Nature Geoscience* 6 (3): 228–34. <https://doi.org/10.1038/ngeo1739>.
- 904 Kendall, Carol. 1998. “USGS -- Isotope Tracers -- Resources: Isotope Tracers in Catchment
905 Hydrology -- Chapter 16.” *Isotope Tracers in Catchment Hydrology Elsevier Science B.V.*
- 906 Khatiwala, S., F. Primeau, and T. Hall. 2009. “Reconstruction of the History of Anthropogenic CO₂
907 Concentrations in the Ocean.” *Nature* 462 (7271): 346–49. <https://doi.org/10.1038/nature08526>.
- 908 Kiefer, D. A., R. J. Olson, and O. Holm-Hansen. 1976. “Another Look at the Nitrite and Chlorophyll
909 Maxima in the Central North Pacific.” *Deep-Sea Research and Oceanographic Abstracts* 23
910 (12). [https://doi.org/10.1016/0011-7471\(76\)90895-0](https://doi.org/10.1016/0011-7471(76)90895-0).
- 911 Kits, K. Dimitri, Christopher J. Sedlacek, Elena V. Lebedeva, Ping Han, Alexandr Bulaev, Petra
912 Pjevac, Anne Daebeler, et al. 2017. “Kinetic Analysis of a Complete Nitrifier Reveals an
913 Oligotrophic Lifestyle.” *Nature* 549 (7671): 269–72. <https://doi.org/10.1038/nature23679>.
- 914 Kitzinger, Katharina, Hannah K. Marchant, Laura A. Bristow, Craig W. Herbold, Cory C. Padilla,
915 Abiel T. Kidane, Sten Littmann, et al. 2020. “Single Cell Analyses Reveal Contrasting Life
916 Strategies of the Two Main Nitrifiers in the Ocean.” *Nature Communications* 11 (1).
917 <https://doi.org/10.1038/s41467-020-14542-3>.
- 918 Kowalchuk, G. A., and J. R. Stephen. 2001. “Ammonia-Oxidizing Bacteria: A Model for Molecular
919 Microbial Ecology.” *Annual Review of Microbiology* 55: 485–529.
920 <https://doi.org/10.1146/annurev.micro.55.1.485>.
- 921 Kozłowski, Jessica A., Michaela Stieglmeier, Christa Schleper, Martin G. Klotz, and Lisa Y. Stein.
922 2016. “Pathways and Key Intermediates Required for Obligate Aerobic Ammonia-Dependent
923 Chemolithotrophy in Bacteria and Thaumarchaeota.” *ISME Journal* 10 (8): 1836–45.
924 <https://doi.org/10.1038/ismej.2016.2>.
- 925 Lomas, Michael W., and Fredric Lipschultz. 2006. “Forming the Primary Nitrite Maximum: Nitrifiers
926 or Phytoplankton?” *Limnology and Oceanography* 51 (5): 2453–67.
927 <https://doi.org/10.4319/lo.2006.51.5.2453>.
- 928 Lückner, Sebastian, Michael Wagner, Frank Maixner, Eric Pelletier, Hanna Koch, Benoit Vacherie,
929 Thomas Rattei, et al. 2010. “A Nitrospira Metagenome Illuminates the Physiology and
930 Evolution of Globally Important Nitrite-Oxidizing Bacteria.” *Proceedings of the National
931 Academy of Sciences of the United States of America* 107 (30): 13479–84.
932 <https://doi.org/10.1073/pnas.1003860107>.
- 933 Martens-Habbena, Willm, Paul M. Berube, Hidetoshi Urakawa, José R. De La Torre, and David A.
934 Stahl. 2009. “Ammonia Oxidation Kinetics Determine Niche Separation of Nitrifying Archaea
935 and Bacteria.” *Nature* 461 (7266): 976–79. <https://doi.org/10.1038/nature08465>.
- 936 Mellvin, Matthew R., and Karen L. Casciotti. 2011. “Technical Updates to the Bacterial Method for

- 937 Nitrate Isotopic Analyses.” *Analytical Chemistry* 83 (5): 1850–56.
938 <https://doi.org/10.1021/ac1028984>.
- 939 Mduityana, Mhlangabezi. 2021. “Mixed Layer Nitrogen Cycling in the Southern Ocean: Seasonality,
940 Kinetics, and Biogeochemical Implications A Thesis Presented for the Degree Of.” *University of*
941 *Cape Town, PhD Thesis*, no. June.
- 942 Mduityana, Mhlangabezi, Xin Sun, Jessica Burger, Raquel Flynn, Shantelle Smith, Natasha R. van
943 Horsten, Eva Bucciarelli, et al. 2022. “The Kinetics of Ammonium Uptake and Oxidation during
944 Winter across the Indian Sector of the Southern Ocean.” *Limnology and Oceanography*, 1–19.
945 <https://doi.org/10.1002/lno.12050>.
- 946 Mduityana, Mhlangabezi, Sandy J. Thomalla, R. Philibert, Bess B. Ward, and Sarah E. Fawcett. 2020.
947 “The Seasonal Cycle of Nitrogen Uptake and Nitrification in the Atlantic Sector of the Southern
948 Ocean.” *Global Biogeochemical Cycles*, no. 3: 1–29. <https://doi.org/10.1029/2019GB006363>.
- 949 Meincke, Michael, Eberhard Bock, Dieter Kastrau, and Peter M.H. Kroneck. 1992. “Nitrite
950 Oxidoreductase from *Nitrobacter Hamburgensis*: Redox Centers and Their Catalytic Role.”
951 *Archives of Microbiology* 158 (2): 127–31. <https://doi.org/10.1007/BF00245215>.
- 952 Milligan, Allen J., and Paul J. Harrison. 2000. “Effects of Non-Steady-State Iron Limitation on
953 Nitrogen Assimilatory Enzymes in the Marine Diatom *Thalassiosira weissflogii*
954 (*Bacillariophyceae*).” *Journal of Phycology* 36 (1): 78–86. <https://doi.org/10.1046/j.1529-8817.2000.99013.x>.
- 956 Monod, Jacques. 1942. “Recherches Sur La Croissance Des Cultures Bacteriennes.” *Hermann and*
957 *Cie, Paris*.
- 958 Mulholland, Margaret R., and Peter W. Bernhardt. 2005. “The Effect of Growth Rate, Phosphorus
959 Concentration, and Temperature on N₂ Fixation, Carbon Fixation, and Nitrogen Release in
960 Continuous Cultures of *Trichodesmium* IMS101.” *Limnology and Oceanography* 50 (3): 839–
961 49. <https://doi.org/10.4319/lo.2005.50.3.0839>.
- 962 Newell, Silvia E., Andrew R. Babbin, Amal Jayakumar, and Bess B. Ward. 2011. “Ammonia
963 Oxidation Rates and Nitrification in the Arabian Sea.” *Global Biogeochemical Cycles* 25 (4): 1–
964 10. <https://doi.org/10.1029/2010GB003940>.
- 965 Newell, Silvia E., Sarah E. Fawcett, and Bess B. Ward. 2013. “Depth Distribution of Ammonia
966 Oxidation Rates and Ammonia-Oxidizer Community Composition in the Sargasso Sea.”
967 *Limnology and Oceanography* 58 (4): 1491–1500. <https://doi.org/10.4319/lo.2013.58.4.1491>.
- 968 Nowka, Boris, Holger Daims, and Eva Spieck. 2015. “Comparison of Oxidation Kinetics of Nitrite-
969 Oxidizing Bacteria : Nitrite Availability as a Key Factor in Niche Differentiation” 81 (2): 745–
970 53. <https://doi.org/10.1128/AEM.02734-14>.
- 971 Olsen, Are, Alex Kozyr, Siv K. Lauvset, Mario Hoppema, Fiz F. Pérez, Reiner Steinfeldt, Sara
972 Jutterström, et al. 2016. “The Global Ocean Data Analysis Project Version 2 (GLODAPv2) – an
973 Internally Consistent Data Product for the World Ocean.” *Earth System Science Data* 8 (2):
974 297–323. <https://doi.org/10.5194/essd-8-297-2016>.
- 975 Olson, RJ. 1981a. “¹⁵N Tracer Studies of the Primary Nitrite Maximum.” *Journal of Marine*
976 *Research* 39 (Number 2): 203–26.
- 977 ———. 1981b. “Differential Photoinhibition of Marine Nitrifying Bacteria - a Possible Mechanism
978 for the Formation of the Primary Nitrite Maximum.” *Journal of Marine Research* 39 (2): 227–
979 38.
- 980 Orsi, H, Thomas Whitworth, and Worth D Nowlin Jr. 1995. “On the Meridional Extent and Fronts of
981 the Antarctic Circumpolar Current Pronounced Meridional Gradients in Surface Properties
982 Separate Waters of the Southern Ocean from the Warmer and Saltier Waters of the Subtropical

- 983 Circulations.” *Deep Sea Research* 42 (5): 641–73. [https://doi.org/10.1016/0967-0637\(95\)00021-](https://doi.org/10.1016/0967-0637(95)00021-)
984 W.
- 985 Pachiadaki, Maria G, Eva Sintes, Kristin Bergauer, Julia M Brown, Nicholas R Record, Brandon K
986 Swan, and Mary Elizabeth Mathyer. 2017. “Major Role of Nitrite-Oxidizing Bacteria in Dark
987 Ocean Carbon Fixation” 1051 (November): 1046–51.
- 988 Pasciak, Walter J, and Jerome Gavis. 1974. “Transport Limitation of Nutrient Uptake in
989 Phytoplankton.” *Limnology and Oceanography* 19 (6): 881–88.
- 990 Peng, Xuefeng, Sarah E. Fawcett, Nicolas van Oostende, Martin J. Wolf, Dario Marconi, Daniel M.
991 Sigman, and Bess B. Ward. 2018. “Nitrogen Uptake and Nitrification in the Subarctic North
992 Atlantic Ocean.” *Limnology and Oceanography*, no. 1967. <https://doi.org/10.1002/lno.10784>.
- 993 Peng, Xuefeng, Clara A. Fuchsman, Amal Jayakumar, Sergey Oleynik, Willm Martens-Habbena,
994 Allan H. Devol, and Bess B. Ward. 2015. “Ammonia and Nitrite Oxidation in the Eastern
995 Tropical North Pacific.” *Global Biogeochemical Cycles* 29 (12): 2034–49.
996 <https://doi.org/10.1002/2015GB005278>.
- 997 Peng, Xuefeng, Clara A. Fuchsman, Amal Jayakumar, Mark J. Warner, Allan H. Devol, and Bess B.
998 Ward. 2016. “Revisiting Nitrification in the Eastern Tropical South Pacific: A Focus on
999 Controls.” *Journal of Geophysical Research: Oceans*. <https://doi.org/10.1002/2015JC011455>.
- 1000 Philibert, R., H. Waldron, and D. Clark. 2015. “A Geographical and Seasonal Comparison of
1001 Nitrogen Uptake by Phytoplankton in the Southern Ocean.” *Ocean Science* 11 (2): 251–67.
1002 <https://doi.org/10.5194/os-11-251-2015>.
- 1003 Pollard, R. T., M. I. Lucas, and J. F. Read. 2002. “Physical Controls on Biogeochemical Zonation in
1004 the Southern Ocean.” *Deep-Sea Research Part II: Topical Studies in Oceanography* 49 (16):
1005 3289–3305. [https://doi.org/10.1016/S0967-0645\(02\)00084-X](https://doi.org/10.1016/S0967-0645(02)00084-X).
- 1006 Qin, Wei, Shady A. Amin, Rachel A. Lundeen, Katherine R. Heal, Willm Martens-Habbena, Serdar
1007 Turkarlan, Hidetoshi Urakawa, et al. 2018. “Stress Response of a Marine Ammonia-Oxidizing
1008 Archaeon Informs Physiological Status of Environmental Populations.” *ISME Journal* 12 (2):
1009 508–19. <https://doi.org/10.1038/ismej.2017.186>.
- 1010 Qin, Wei, Shady A. Amin, Willm Martens-Habbena, Christopher B. Walker, Hidetoshi Urakawa,
1011 Allan H. Devol, Anitra E. Ingalls, James W. Moffett, E. Virginia Armbrust, and David A. Stahl.
1012 2014. “Marine Ammonia-Oxidizing Archaeal Isolates Display Obligate Mixotrophy and Wide
1013 Ecotypic Variation.” *Proceedings of the National Academy of Sciences of the United States of*
1014 *America* 111 (34): 12504–9. <https://doi.org/10.1073/pnas.1324115111>.
- 1015 Raven, J. A., and P. G. Falkowski. 1999. “Oceanic Sinks for Atmospheric CO₂.” *Plant, Cell and*
1016 *Environment* 22 (6): 741–55. <https://doi.org/10.1046/j.1365-3040.1999.00419.x>.
- 1017 Read, J. F., R. T. Pollard, and U. Bathmann. 2002. “Physical and Biological Patchiness of an Upper
1018 Ocean Transect from South Africa to the Ice Edge near the Greenwich Meridian.” *Deep-Sea*
1019 *Research Part II: Topical Studies in Oceanography* 49 (18): 3713–33.
1020 [https://doi.org/10.1016/S0967-0645\(02\)00108-X](https://doi.org/10.1016/S0967-0645(02)00108-X).
- 1021 Rees, Andrew P., Ian Joint, and Kirsten M. Donald. 1999. “Early Spring Bloom Phytoplankton-
1022 Nutrient Dynamics at the Celtic Sea Shelf Edge.” *Deep-Sea Research Part I: Oceanographic*
1023 *Research Papers*. [https://doi.org/10.1016/S0967-0637\(98\)00073-9](https://doi.org/10.1016/S0967-0637(98)00073-9).
- 1024 Saito, Mak A., Matthew R. McIlvin, Dawn M. Moran, Alyson E. Santoro, Chris L. Dupont, Patrick A.
1025 Rafter, Jaclyn K. Saunders, et al. 2020. “Abundant Nitrite-Oxidizing Metalloenzymes in the
1026 Mesopelagic Zone of the Tropical Pacific Ocean.” *Nature Geoscience* 13 (5): 355–62.
1027 <https://doi.org/10.1038/s41561-020-0565-6>.
- 1028 Santoro, A. E., C. M. Sakamoto, J. M. Smith, J. N. Plant, A. L. Gehman, A. Z. Worden, K. S.

- 1029 Johnson, C. A. Francis, and K. L. Casciotti. 2013. "Measurements of Nitrite Production in and
1030 around the Primary Nitrite Maximum in the Central California Current." *Biogeosciences* 10
1031 (11): 7395–7410. <https://doi.org/10.5194/bg-10-7395-2013>.
- 1032 Santoro, Alyson E., Christopher L. Dupont, R. Alex Richter, Matthew T. Craig, Paul Carini, Matthew
1033 R. McIlvin, Youngik Yang, William D. Orsi, Dawn M. Moran, and Mak A. Saito. 2015.
1034 "Genomic and Proteomic Characterization of 'Candidatus Nitrosopelagicus Brevis': An
1035 Ammonia-Oxidizing Archaeon from the Open Ocean." *Proceedings of the National Academy of
1036 Sciences of the United States of America* 112 (4): 1173–78.
1037 <https://doi.org/10.1073/pnas.1416223112>.
- 1038 Schaefer, Sylvia C., and James T. Hollibaugh. 2017. "Temperature Decouples Ammonium and Nitrite
1039 Oxidation in Coastal Waters." *Environmental Science and Technology* 51 (6): 3157–64.
1040 <https://doi.org/10.1021/acs.est.6b03483>.
- 1041 Schofield, Oscar, Travis Miles, Anne Carlijn Alderkamp, Sang Hoon Lee, Christina Haskins, Emily
1042 Rogalsky, Rachel Sipler, Robert M. Sherrell, and Patricia L. Yager. 2015. "In Situ
1043 Phytoplankton Distributions in the Amundsen Sea Polynya Measured by Autonomous Gliders."
1044 *Elementa*. <https://doi.org/10.12952/journal.elementa.000073>.
- 1045 Sciandra, A., and R. Amara. 1994. "Effects of Nitrogen Limitation on Growth and Nitrite Excretion
1046 Rates of the Dinoflagellate *Prorocentrum Minimum*." *Marine Ecology Progress Series* 105 (3):
1047 301. <https://doi.org/10.3354/meps105301>.
- 1048 Shafiee, Roxana T., Joseph T. Snow, Qiong Zhang, and Rosalind E. M. Rickaby. 2019. "Iron
1049 Requirements and Uptake Strategies of the Globally Abundant Marine Ammonia-Oxidising
1050 Archaeon, *Nitrosopumilus Maritimus* SCM1." *The ISME Journal*.
1051 <https://doi.org/10.1038/s41396-019-0434-8>.
- 1052 Sigman, D. M., K. L. Casciotti, M. Andreani, C. Barford, M. Galanter, and J. K. Böhlke. 2001. "A
1053 Bacterial Method for the Nitrogen Isotopic Analysis of Nitrate in Seawater and Freshwater."
1054 *Analytical Chemistry* 73 (17): 4145–53. <https://doi.org/10.1021/ac010088e>.
- 1055 Smart, Sandi M, Sarah E Fawcett, Sandy J Thomalla, Mira a Weigand, Chris J C Reason, and Daniel
1056 M Sigman. 2015. "Global Biogeochemical Cycles," 1–19.
1057 <https://doi.org/10.1002/2014GB005013>.Received.
- 1058 Smith, Shantelle, Katye E. Altieri, Mhlangabezi Mduyana, David R. Walker, Ruan G. Parrott, Sedick
1059 Gallie, Kurt A.M. Spence, Jessica M. Burger, and Sarah E. Fawcett. 2022. "Biogeochemical
1060 Controls on Ammonium Accumulation in the Surface Layer of the Southern Ocean."
1061 *Biogeosciences* 19 (3): 715–41. <https://doi.org/10.5194/bg-19-715-2022>.
- 1062 Sorokin, Dimitry Y., Sebastian Lücker, Dana Vejmelkova, Nadezhda A. Kostrikina, Robbert
1063 Kleerebezem, W. Irene C. Rijpstra, Jaap S. Sinninghe Damsté, et al. 2012. "Nitrification
1064 Expanded: Discovery, Physiology and Genomics of a Nitrite-Oxidizing Bacterium from the
1065 Phylum Chloroflexi." *ISME Journal* 6 (12): 2245–56. <https://doi.org/10.1038/ismej.2012.70>.
- 1066 Spieck, Eva, Silke Ehrich, and Jens Aamand. 1998. "Isolation and Immunocytochemical Location of
1067 the Nitrite-Oxidizing System in *Nitrospira Moscoviensis*." *Arch Microbiol*, no. 169: 225–30.
- 1068 Sun, Xin, Claudia Frey, Emilio Garcia-Robledo, Amal Jayakumar, and Bess B. Ward. 2021.
1069 "Microbial Niche Differentiation Explains Nitrite Oxidation in Marine Oxygen Minimum
1070 Zones." *The ISME Journal*, 1–13. <https://doi.org/10.1038/s41396-020-00852-3>.
- 1071 Sun, Xin, Qixing Ji, Amal Jayakumar, and Bess B. Ward. 2017. "Dependence of Nitrite Oxidation on
1072 Nitrite and Oxygen in Low-Oxygen Seawater." *Geophysical Research Letters* 44 (15): 7883–91.
1073 <https://doi.org/10.1002/2017GL074355>.
- 1074 Sundermeyer-Klinger, Hilke, Wolfgang Meyer, Beate Warninghoff, and Eberhard Bock. 1984.

- 1075 “Membrane-Bound Nitrite Oxidoreductase of Nitrobacter: Evidence for a Nitrate Reductase
1076 System.” *Archives of Microbiology* 140 (2–3). <https://doi.org/10.1007/BF00454918>.
- 1077 Tagliabue, A., T. Mtshali, O. Aumont, A. R. Bowie, M. B. Klunder, A. N. Roychoudhury, and S.
1078 Swart. 2012. “A Global Compilation of Dissolved Iron Measurements: Focus on Distributions
1079 and Processes in the Southern Ocean.” *Biogeosciences* 9 (6): 2333–49.
1080 <https://doi.org/10.5194/bg-9-2333-2012>.
- 1081 Tsoularis, A, and J Wallace. 2002. “Analysis of Logistic Growth Models.” *Mathematical Biosciences*
1082 179: 21–55.
- 1083 Ushiki, Norisuke, Masaru Jinno, Hirotugu Fujitani, Toshikazu Suenaga, Akihiko Terada, and Satoshi
1084 Tsuneda. 2017. “Nitrite Oxidation Kinetics of Two Nitrospira Strains : The Quest for
1085 Competition and Ecological Niche Differentiation.” *Journal of Bioscience and Bioengineering*
1086 123 (5): 581–89. <https://doi.org/10.1016/j.jbiosc.2016.12.016>.
- 1087 Vaccaro, Ralph F, and John H Ryther. 1960. “Marine Phytoplankton and the Distribution of Nitrite in
1088 the Sea*.” *ICES Journal of Marine Science* 25 (3): 260–71.
1089 <https://doi.org/10.1093/icesjms/25.3.260>.
- 1090 Vajrала, Neeraja, Willm Martens-Habben, Luis A. Sayavedra-Soto, Andrew Schauer, Peter J.
1091 Bottomley, David A. Stahl, and Daniel J. Arp. 2013. “Hydroxylamine as an Intermediate in
1092 Ammonia Oxidation by Globally Abundant Marine Archaea.” *Proceedings of the National*
1093 *Academy of Sciences of the United States of America* 110 (3): 1006–11.
1094 <https://doi.org/10.1073/pnas.1214272110>.
- 1095 Volk, T., and M. I. Hoffert. 1985. “Ocean Carbon Pumps: Analysis of Relative Strengths and
1096 Efficiencies in Ocean-Driven Atmospheric CO₂ Changes.” *The Carbon Cycle and Atmospheric*
1097 *CO₂*.
- 1098 Walker, C. B., J. R. De La Torre, M. G. Klotz, H. Urakawa, N. Pinel, D. J. Arp, C. Brochier-Armanet,
1099 et al. 2010. “Nitrosopumilus Maritimus Genome Reveals Unique Mechanisms for Nitrification
1100 and Autotrophy in Globally Distributed Marine Crenarchaea.” *Proceedings of the National*
1101 *Academy of Sciences of the United States of America* 107 (19): 8818–23.
1102 <https://doi.org/10.1073/pnas.0913533107>.
- 1103 Ward, B. B. 2005. “Temporal Variability in Nitrification Rates and Related Biogeochemical Factors
1104 in Monterey Bay, California, USA.” *Marine Ecology Progress Series* 292: 97–109.
1105 <https://doi.org/10.3354/meps292097>.
- 1106 ———. 2008. “Chapter 5 - Nitrification in Marine Systems.” In *Nitrogen in the Marine Environment*
1107 *(2nd Edition)*, 199–261. <https://doi.org/http://dx.doi.org/10.1016/B978-0-12-372522-6.00005-0>.
- 1108 Ward, B. B., and K. A. Kilpatrick. 1991. “Nitrogen Transformations in the Oxidic Layer of Permanent
1109 Anoxic Basins: The Black Sea and the Cariaco Trench.” In *Black Sea Oceanography*.
1110 https://doi.org/10.1007/978-94-011-2608-3_7.
- 1111 Ward, B. B., and O. C. Zafiriou. 1988. “Nitrification and Nitric Oxide in the Oxygen Minimum of the
1112 Eastern Tropical North Pacific.” *Deep Sea Research Part A, Oceanographic Research Papers*
1113 35 (7): 1127–42. [https://doi.org/10.1016/0198-0149\(88\)90005-2](https://doi.org/10.1016/0198-0149(88)90005-2).
- 1114 Watson, Andrew J., Ute Schuster, Jamie D. Shutler, Thomas Holding, Ian G.C. Ashton, Peter
1115 Landschützer, David K. Woolf, and Lonneke Goddijn-Murphy. 2020. “Revised Estimates of
1116 Ocean-Atmosphere CO₂ Flux Are Consistent with Ocean Carbon Inventory.” *Nature*
1117 *Communications* 11 (1): 1–6. <https://doi.org/10.1038/s41467-020-18203-3>.
- 1118 Watson, Stanley W., Eberhard Bock, Frederica W. Valois, John B. Waterbury, and Ursula Schlosser.
1119 1986. “Nitrospira Marina Gen. Nov. Sp. Nov.: A Chemolithotrophic Nitrite-Oxidizing
1120 Bacterium.” *Archives of Microbiology*. <https://doi.org/10.1007/BF00454947>.

1121 Watson, Stanley W., and John B. Waterbury. 1971. "Characteristics of Two Marine Nitrite Oxidizing
1122 Bacteria,," *Microscopy* 77 (2631): 203–30.

1123 Weigand, M. Alexandra, Julien Foriel, Bruce Barnett, Sergey Oleynik, and Daniel M. Sigman. 2016.
1124 "Updates to Instrumentation and Protocols for Isotopic Analysis of Nitrate by the Denitrifier
1125 Method." *Rapid Communications in Mass Spectrometry* 30 (12): 1365–83.
1126 <https://doi.org/10.1002/rcm.7570>.

1127 Xu, Min Nina, Xiaolin Li, Dalin Shi, Yao Zhang, Minhan Dai, Tao Huang, Patricia M. Glibert, and
1128 Shuh Ji Kao. 2019. "Coupled Effect of Substrate and Light on Assimilation and Oxidation of
1129 Regenerated Nitrogen in the Euphotic Ocean." *Limnology and Oceanography* 64 (3): 1270–83.
1130 <https://doi.org/10.1002/lno.11114>.

1131 Yool, Andrew, Adrian P Martin, Camila Fernández, and Darren R Clark. 2007. "The Significance of
1132 Nitrification for Oceanic New Production." *Nature* 447 (7147): 999–1002.
1133 <https://doi.org/10.1038/nature05885>.

1134 Zakem, Emily J., Alia Al-Haj, Matthew J. Church, Gert L. Van Dijken, Stephanie Dutkiewicz, Sarah
1135 Q. Foster, Robinson W. Fulweiler, Matthew M. Mills, and Michael J. Follows. 2018.
1136 "Ecological Control of Nitrite in the Upper Ocean." *Nature Communications* 9 (1).
1137 <https://doi.org/10.1038/s41467-018-03553-w>.

1138 Zhang, Yao, Wei Qin, Lei Hou, Emily J. Zakem, Xianhui Wan, Zihao Zhao, Li Liu, et al. 2020.
1139 "Nitrifier Adaptation to Low Energy Flux Controls Inventory of Reduced Nitrogen in the Dark
1140 Ocean." *Proceedings of the National Academy of Sciences of the United States of America* 117
1141 (9): 4823–30. <https://doi.org/10.1073/pnas.1912367117>.

1142

1143

1144

1145

1146

1147

1148

1149

1150

1151

1152

1153

1154

1155

1156

1157

1158

1159

1160 **Tables and figures**

1161 **Table 1:** Kinetic parameters (V_{\max} , K_m , and C) associated with NO_2^- oxidation experiments conducted
 1162 across the western Indian sector of the Southern Ocean in winter 2017. Included here is the best fit and
 1163 95% confidence interval (“CI”) for each kinetic parameter, derived using a non-linear, least-squares
 1164 optimization method (Scipy lmfit package, Python 3.7.6).

Station name	Latitude	Longitude	$[\text{NO}_2^-]_{\text{amb}}$ (nM)	V_{\max} (nM d ⁻¹)	95%CI (nM d ⁻¹)	K_m (nM)	95%CI (nM)	C (nM)	95%CI (nM)
St 01	37°S	19°E	157	9.1	7.9 to 10	263	192 to 350	193	144 to 206
St 02	42°S	21°E	108	5.2	4.8 to 5.5	134	109 to 163	115	105 to 119
St 03	45°S	22°E	103	8.3	7.4 to 9.3	206	15 to 373	139	-11 to 163
St 04	50°S	26°E	162	13	11 to 15	288	104 to 538	172	68 to 204
St 05	55°S	28°E	212	14	13 to 15	329	183 to 458	245	138 to 272
St 06	62°S	30°E	226	8.2	7.8 to 8.6	403	320 to 499	163	129 to 187
St 07	62°S	30°E	226	6.6	6.0 to 7.4	317	234 to 395	237	190 to 255

1165

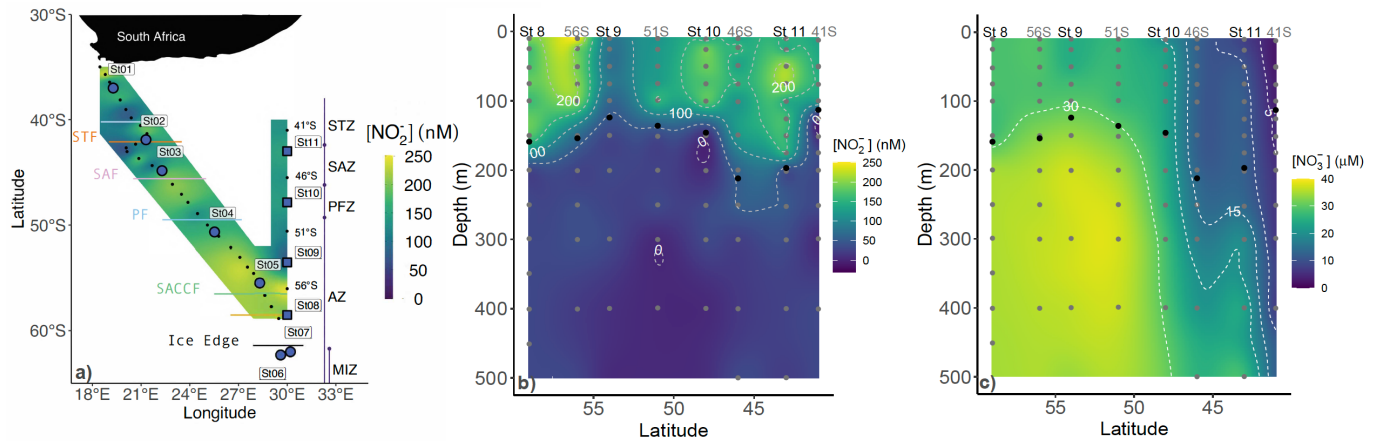
1166 **Table 2:** A selection of previously derived K_m and V_{\max} values from the open ocean, along with the
 1167 concurrently-measured ambient concentrations of nitrite ($[\text{NO}_2^-]_{\text{amb}}$). The numbers in parenthesis are
 1168 standard errors.

Region	$[\text{NO}_2^-]$ (nM)	Sampled depth (m)	K_m (nM)	V_{\max} (nM d ⁻¹)	Reference
Indian Southern Ocean: St 01: 37°S	157	7	263 (16)	9.1 (0.5)	This study
Indian Southern Ocean: St 02: 42°S	108	7	134 (8)	5.2 (0.1)	This study
Indian Southern Ocean: St 03: 45°S	103	7	206 (30)	8.3 (0.4)	This study
Indian Southern Ocean: St 04: 51°S	162	7	288 (52)	13 (0.7)	This study
Indian Southern Ocean: St 05: 56°S	212	7	329 (29)	14 (0.4)	This study
Indian Southern Ocean: St 06: 62°S	226	7	403 (24)	8.2 (0.1)	This study
Indian Southern Ocean: St 07: 62°S	226	7	317 (20)	6.6 (0.3)	This study
Southern California Bight	20	60	70	nd	Olson 1981
Eastern Tropical North Pacific	100	53	281 (151)	63 (14)	Sun et al. 2017
Eastern Tropical North Pacific	50	170	227 (55)	56 (5.4)	Sun et al. 2017
South China Sea	51	110	195 (33)	30 (1.6)	Zhang et al. 2020
South China Sea	71	95	175 (37)	24 (1.5)	Zhang et al. 2020
South China Sea	31	150	49 (15)	9.6 (0.6)	Zhang et al. 2020
South China Sea	185	75	506 (82)	12 (0.8)	Zhang et al. 2020
South China Sea	34	200	27 (11)	4.6 (0.3)	Zhang et al. 2020
Subtropical South Atlantic	14	150	74 (29)	22 (0.7)	Fawcett et al. unpubl
Subtropical South Atlantic	152	150	167 (4.3)	27 (0.2)	Fawcett et al. unpubl

nd represents not determined

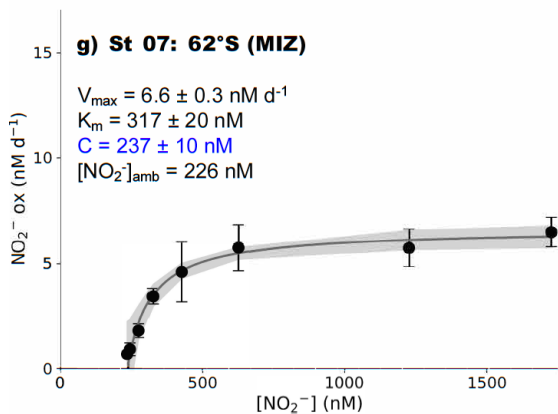
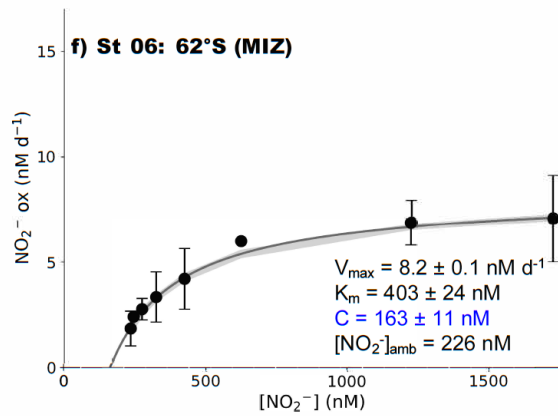
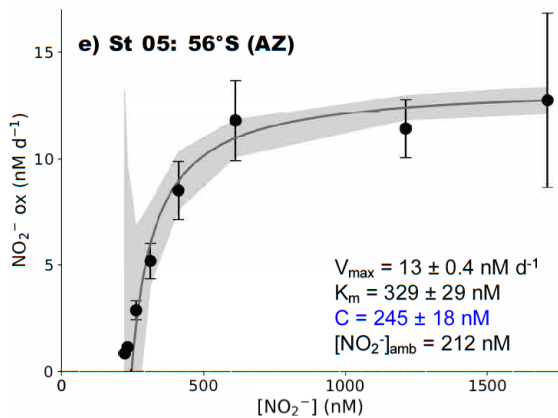
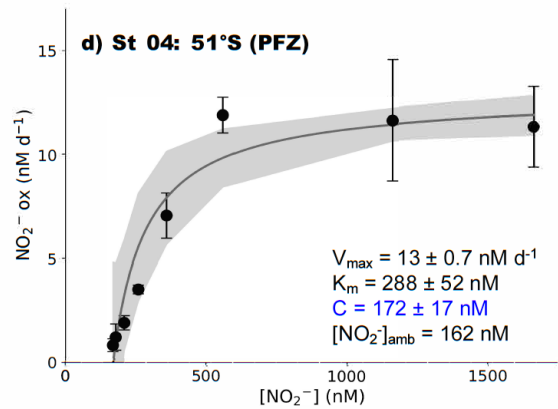
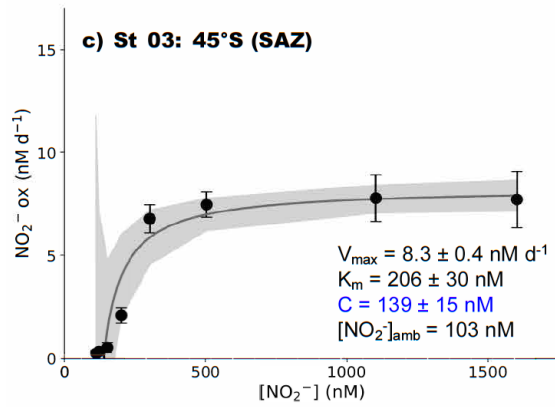
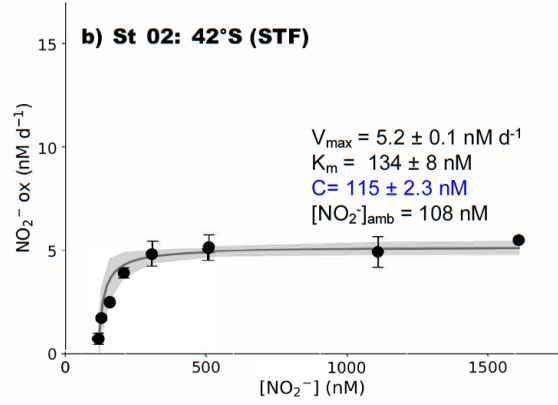
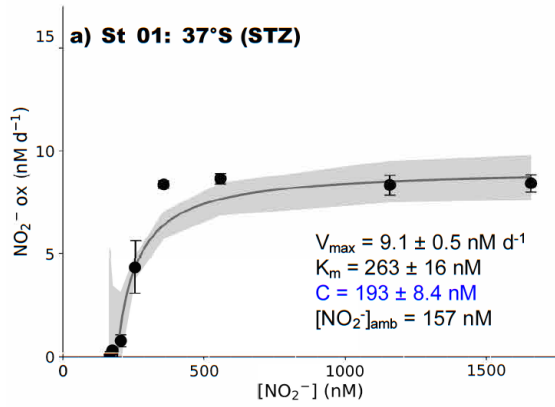
1169

1170

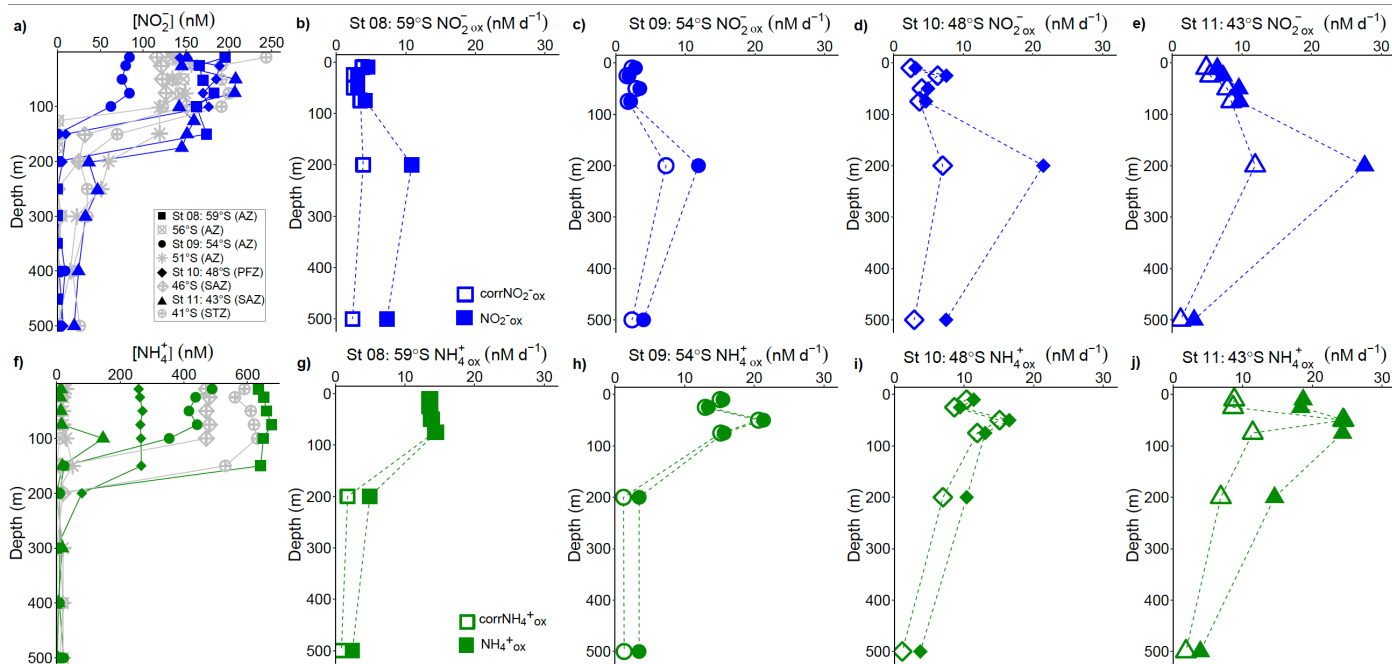


1171

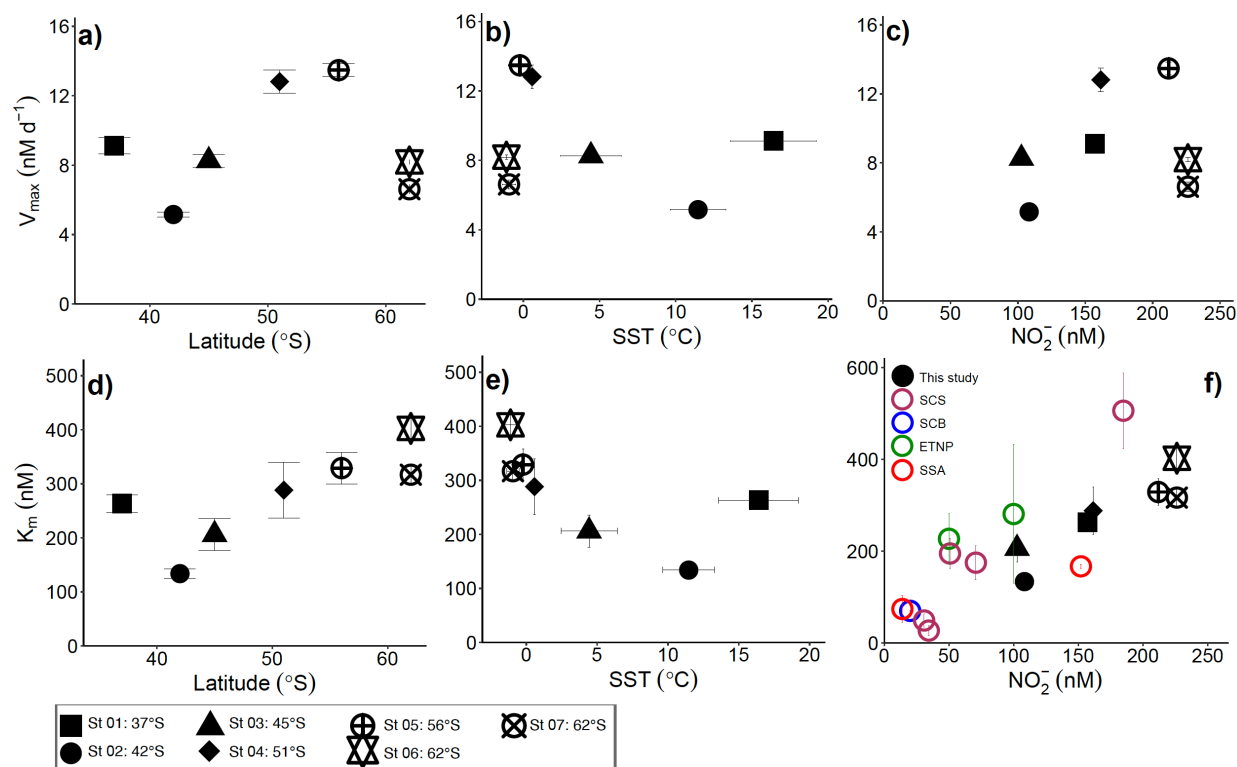
1172 **Figure 1:** a) Map of the cruise track showing the kinetics stations (large circle symbols) and locations
 1173 of the underway stations sampled during Leg 1 (small symbols), overlaid on the measured surface (~7
 1174 m) nitrite concentrations ($[\text{NO}_2^-]$). Additionally, the locations of the hydrocast stations occupied during
 1175 Leg 2 are shown, with the stations at which depth-profile experiments were conducted shown by the
 1176 large square symbols. The coloured horizontal lines denote the frontal positions at the time of sampling
 1177 and the major zones of the Southern Ocean are indicated by the vertical lines and dots – STZ,
 1178 Subtropical Zone; STF, Subtropical Front; SAZ, Subantarctic Zone; SAF, Subantarctic Front; PFZ,
 1179 Polar Frontal Zone; PF, Polar Front; AZ, Antarctic Zone; SACCF, Southern Antarctic Circumpolar
 1180 Front; MIZ, Marginal Ice Zone. Also shown are water column (0-500 m) profiles of the concentrations
 1181 of b) nitrite (NO_2^-) and c) nitrate (NO_3^-) sampled during Leg 2. The grey dots indicate the discrete
 1182 sampling depths at all the hydrocast stations (eight in total), with the four stations at which depth profile
 1183 experiments were conducted (St 08 to St 11) labeled above the panel. The black dots show the derived
 1184 mixed layer depths.



1186 **Figure 2:** Kinetics experiments: the dependence of the NO_2^- oxidation rates on NO_2^- concentration
 1187 ($[\text{NO}_2^-]$) at the surface (~ 7 m) in winter at a) St 01: 37°S (STZ), b) St 02: 42°S (STF), c) St 03: 45°S
 1188 (SAZ), d) St 04: 51°S (PFZ), e) St 05: 55°S (OAZ), f) St 06: 62°S (MIZ), and g) St 07: 62°S (MIZ).
 1189 The solid lines show the Michaelis-Menten best fit, with the derived values of V_{max} , K_m , and C , as well
 1190 as the ambient concentration of nitrite ($[\text{NO}_2^-]_{\text{amb}}$), indicated on each panel. Error bars represent the
 1191 range of values, each measured at least twice. Where errors bars are not visible, they are smaller than
 1192 the data markers. The grey shaded area shows the 95% confidence interval associated with the model
 1193 fit. Note that the x-axis represents total $[\text{NO}_2^-]$ (i.e., $[\text{NO}_2^-]_{\text{tracer}} + [\text{NO}_2^-]_{\text{amb}}$).
 1194

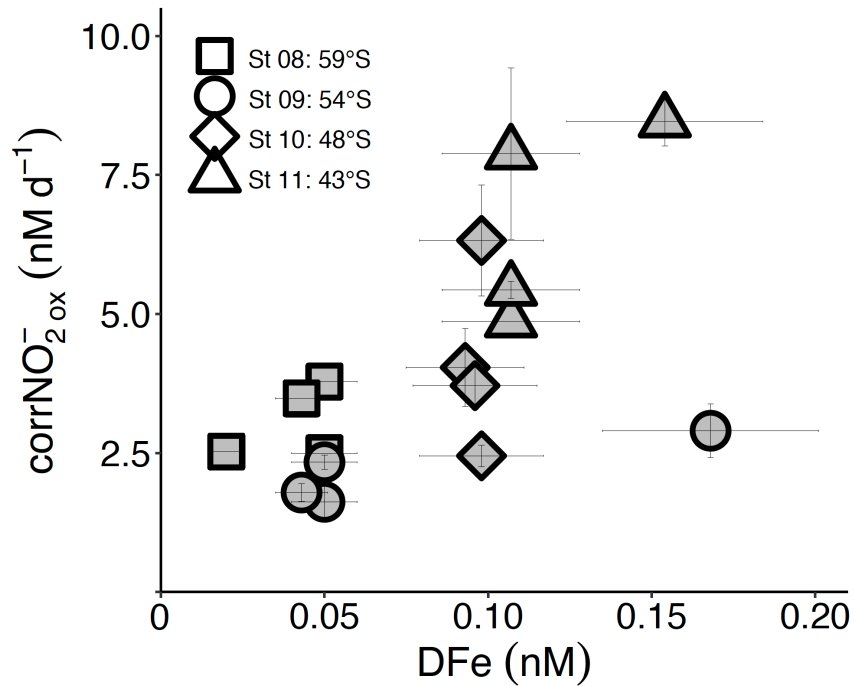


1195 **Figure 3:** Depth-profile experiments: water column (0-500 m) profiles of the concentration of a) nitrite
 1196 ($[\text{NO}_2^-]$) and f) ammonium ($[\text{NH}_4^+]$), and rates of NO_2^- and NH_4^+ oxidation at b and g) St 08: 59°S (AZ),
 1197 c and h) St 09: 54°S (AZ), d and i) St 10: 48°S (PFZ), and e and j) St 11: 43°S (SAZ). In panels a and
 1198 f, the blue and green symbols indicate the stations at which oxidation rates were measured while the
 1199 grey symbols show data from the stations where no experiments were conducted. In panels b-e and g-
 1200 j, open symbols show the oxidation rates revised for possible stimulation due to ^{15}N -tracer additions
 1201 (corr NO_2^- ox and corr NH_4^+ ox; equation 4) and closed symbols show the uncorrected rates (equation 1).
 1202 Error bars indicate the range of values, each measured at least twice. Where error bars are not visible,
 1203 they are smaller than the data markers. The dashed lines connecting the data points are included only to
 1204 guide the eye and should not be taken to imply interpolation with depth.
 1205



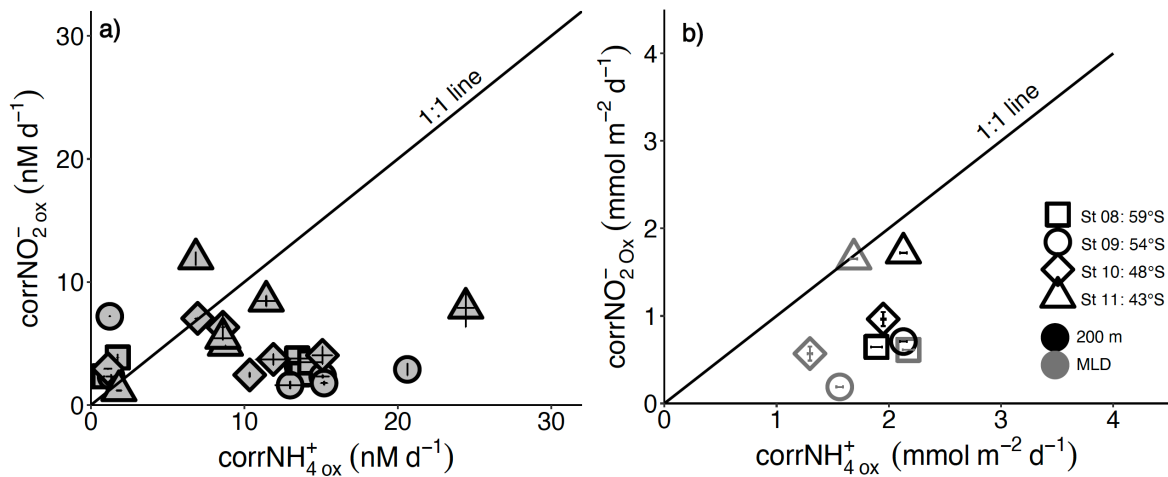
1206

1207 **Figure 4:** Potential controls on the kinetic parameters associated with NO_2^- oxidation. V_{max} and K_m are
 1208 shown as a function of a and d) latitude, b and e) sea surface temperature (SST), and c and f) the ambient
 1209 nitrite concentration ($[NO_2^-]_{amb}$). Vertical error bars show the propagated error associated with V_{max} and
 1210 K_m computed using a non-linear, least-squares optimization method (Scipy lmfit package, Python
 1211 3.7.6), while the symbols and horizontal error bars on panels b and e indicate the average (± 1 standard
 1212 deviation) SST experienced by the sampled communities during the incubations. In panel f, black
 1213 symbols show our Southern Ocean data, maroon symbols show K_m values from the South China Sea
 1214 (SCS; Zhang et al. 2020), the blue symbol shows the K_m value derived for the South California Bight
 1215 (SCB; Olson 1981a), the green symbol shows K_m values from Eastern Tropical North Pacific oxygen
 1216 deficient zone (ETNP; Sun et al. 2017), and the red symbols show K_m values derived for the subtropical
 1217 southeast Atlantic (SSA; Fawcett et al. unpubl.).



1218
1219
1220
1221
1222
1223

Figure 5: Euphotic zone (0-75 m) revised rates of NO_2^- oxidation ($\text{corrNO}_2^-_{\text{ox}}$) measured at the depth-profile stations (St 08 to St 11) plotted against coincident dissolved iron concentrations (DFe). Error bars indicate the range of values, each measured at least twice. Where error bars are not visible, they are smaller than the data markers.



1224
1225
1226
1227
1228
1229
1230
1231
1232

Figure 6: The relationship between the revised rates of NO_2^- and NH_4^+ oxidation ($\text{corrNO}_2^-_{\text{ox}}$ and $\text{corrNH}_4^+_{\text{ox}}$) for a) each experiment depth in the upper water column (0-500 m) and b) integrated over the mixed layer (grey symbols) and upper 200 m (black symbols). Error bars on panel a indicate the range of values, each measured at least twice, while on panel b, error bars show the propagated error. Where error bars are not visible, they are smaller than the data markers. The black diagonal line on both panels has a slope of 1, which is expected if the rates of NH_4^+ and NO_2^- oxidation are tightly coupled.